



Leptothrix discophora SP-6 : effects of biofilms on passive film chemistry of 316L stainless steel and modeling of growth  
by Nurdan Yurt

A dissertation submitted in partial fulfillment of the requirements for the degree of Doctor of Philosophy in Chemical Engineering  
Montana State University  
© Copyright by Nurdan Yurt (2002)

**Abstract:**

This thesis examined effects of manganese oxidizing bacteria, *Leptothrix discophora* SP-6 biofilms, on passive film chemistry and pitting corrosion of 316L stainless steel..

Biofilms of manganese oxidizing bacteria attach to the passive films of metals and deposit manganese oxides on the surfaces. These oxides, being in equilibrium with manganese ions in water, shift the corrosion potential of the passive metals in the noble direction, causing a phenomenon known as “ennoblement”. Ennoblement is of interest because it increases corrosion potential, which may initiate localized forms of corrosion of passive metals, pitting corrosion. The mechanism of pit initiation on the ennobled coupons still is not completely known. For localized corrosion to occur, the passive film has to be broken down, and it has been speculated that the biofilms of manganese oxidizing bacteria have a direct effect on the chemistry of the passive films.

The effect of ennoblement of 316L stainless steel by biomineralized manganese deposits on chemistry of passive films was studied using surface-sensitive analytical techniques and cyclic polarization. Depth profiles of elements in the passive films on the ennobled coupons were analyzed using x-ray photoelectron spectroscopy (XPS), and distribution of metal elements were examined by time-of-flight secondary ion mass spectroscopy (ToFSIMS). The results showed that oxide layers on the ennobled coupons were thinner than those on the control coupons.. Cyclic polarization curves showed that ennobled 316L stainless steel indicated, significant loss of passivity. It was concluded that metabolic activity of manganese oxidizing bacteria, *Leptothrix discophora* SP-6 degraded the quality of the passive film on stainless steel coupons by locally reducing its thickness and lowering the pitting potential.

To relate the kinetics of ennoblement to the rate of deposition of manganese oxides on metal surfaces, growth kinetics of *Leptothrix discophora* SP-6 were quantified in biofilms and in planktonic form. In planktonic form, double-substrate growth kinetics, using Monod growth kinetics for pyruvate and Tessier growth kinetics for oxygen, showed the best agreement with the experimental data. Monod model of microbial growth kinetics adequately represents the growth of *Leptothrix discophora* SP-6 biofilms.

*LEPTOTHRIX DISCOPHORA* SP-6: EFFECTS OF  
BIOFILMS ON PASSIVE FILM CHEMISTRY OF 316L  
STAINLESS STEEL AND MODELING OF GROWTH

by

Nurdan Yurt

A dissertation submitted in partial fulfillment of the  
requirements for the degree

of

Doctor of Philosophy

in

Chemical Engineering

MONTANA STATE UNIVERSITY  
Bozeman, Montana

May 2002

© COPYRIGHT

by

Nurdan Yurt

2002

All Rights Reserved

D378  
4928

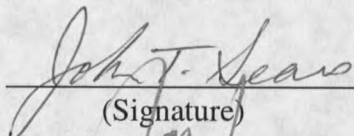
APPROVAL

of a dissertation submitted by

Nurdan Yurt

This dissertation has been read by each member of the dissertation committee and has been found to be satisfactory regarding content, English usage, format, citations, bibliographic style, and consistency, and is ready for submission to the College of Graduate Studies.

Dr. John Sears  
(Chair Person)

  
(Signature)

May 10, 2002  
Date

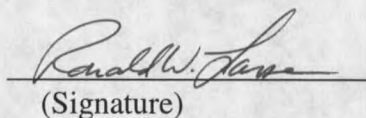
Dr. Zbigniew Lewandowski  
(Chair Person)

  
(Signature)

05/13/02  
Date

Approval for the Department of Chemical Engineering

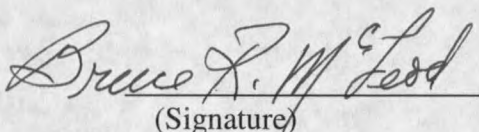
Dr. Ron Larsen

  
(Signature)

5/13/02  
Date

Approval for the College of Graduate Studies

Dr. Bruce McLeod

  
(Signature)

5-20-02  
Date

## STATEMENT OF PERMISSION TO USE

In presenting this dissertation in partial fulfillment of the requirement for a doctoral degree at Montana State University, I agree that the Library shall make it available to borrowers under rules of the Library. I further agree that copying of this dissertation is allowable only for scholarly purposes, consistent with "fair use" as prescribed in the U.S. Copyright Law. Requests for extensive copying or reproduction of this dissertation should be referred to Bell & Howell Information and Learning, 300 North Zeeb Road, Ann Arbor, Michigan 48106, to whom I have granted "the exclusive right to reproduce and distribute my dissertation in and from a microform along with the non-exclusive right to reproduce and distribute my abstract in any format in whole or in part."

Signature 

Date 05/13/2002

## ACKNOWLEDGEMENT

I am thankful to my advisors Zbigniew Lewandowski, Recep Avci and John T. Sears for their guidance and interest in my research. Their support, knowledge and encouragement have helped a lot in completion of this thesis. I thank also to the remaining committee members Phil Stewart and Eric Grimsrud who were always available for my questions and discussion.

I appreciate all faculty, staff and students at the Center for Biofilm Engineering who contributed to my research. Special thanks go to our lab manager, John Neuman for his help and incredible patience during my research.

I would like to specially thank the ICAL facility for the use of XPS and ToFSIMS.

My appreciation goes to my husband, Haluk Beyenal for his continuous encouragements and support. I could not have finished this thesis without the love of Haluk and our son, Cem M. Beyenal. My parents and sisters deserve many thanks for their infinite love.

This work was supported by United States Office Naval Research, contract number N00014-99-1-0701 and by Cooperative Agreement EEC-8907039 between the National Science Foundation and Montana State University, Bozeman, MT, USA.

## TABLE OF CONTENTS

1. INTRODUCTION .....	1
Manganese biomineralization on stainless steel .....	4
Stainless steels .....	4
Pitting corrosion .....	5
Passive film breakdown .....	5
Metastable pitting .....	9
Pit growth .....	10
Manganese biomineralization and manganese cycle .....	10
Role of passive layer during manganese biomineralization on stainless steel surface .....	14
Hypothesis 1 .....	15
Hypothesis 2 .....	15
Biokinetics of microorganism growth .....	17
Microbial growth .....	17
Microbial growth kinetics .....	19
Multiple substrate limited growth .....	22
Substrate utilization rate .....	22
Determination of microbial growth kinetics .....	23
<i>Leptothrix discophora</i> SP-6 .....	24
Growth kinetics of <i>Leptothrix discophora</i> SP-6 .....	26
Hypothesis 3 .....	26
Biofilm growth .....	26
Microbial growth in biofilms .....	28
Hypothesis 4 .....	34
Hypothesis 5 .....	34
Experimental methods .....	35
Passive film examination .....	35
Stainless steel coupon preparation .....	35
Ennoblement experiments .....	36
Coupon classifications for different experiments .....	39
XPS analysis .....	40
ToF-SIMS experiments .....	41
Measurement of pitting corrosion .....	41
Planktonic growth kinetic measurements .....	46
Chemostat .....	46
Biofilm growth kinetic measurements .....	47
Colony biofilms .....	47
Dissolved oxygen microelectrode measurements .....	49

2. BIOMINERALIZED MANGANESE DEGRADES PASSIVE FILMS AND LOWERS PITTING POTENTIAL OF STAINLESS STEEL 316L .....	52
Abstract .....	53
Introduction .....	54
Materials and methods .....	56
Ennoblement experiments .....	56
XPS analysis .....	60
ToF-SIMS analysis .....	60
Cyclic polarizations .....	61
Results and discussion .....	62
XPS analysis .....	62
Stainless steel coupons with removed biomineral deposits ..	62
Stainless steel coupons with intact biomineral deposits .....	62
ToF-SIMS results .....	78
Pitting potentials .....	80
Conclusions .....	84
3. MULTIPLE SUBSTRATE GROWTH KINETICS OF	
<i>Leptothrix discophora</i> SP-6 .....	85
Abstract .....	86
Introduction .....	87
Materials and methods .....	88
Microorganisms .....	88
Chemostat .....	89
Analytical methods .....	92
Selecting the growth model and estimating the kinetic constant .....	94
Maintenance and yield factors .....	95
Non-linear regression to calculate biokinetic parameters .....	96
Selecting the best model and running sensitivity analysis .....	98
Results and discussion .....	99
Modeling growth kinetics .....	101
Tessier's growth model and half rate constant for oxygen .....	104
Maintenance coefficients and yield factors .....	106
Conclusions .....	108
4. BIOKINETIC PARAMETERS FOR MICROBIAL GROWTH IN BIOFILMS QUANTIFIED FROM SUBSTRATE CONCENTRATION PROFILES ....	109
Abstract .....	110
Introduction .....	111
Materials and methods .....	114
Biofilms .....	114

Microelectrode measurements.....	116
An example of the measured profiles.....	117
Mathematical model.....	119
Microbial growth and substrate consumption .....	119
Solution algorithm.....	122
Calculation of confidence limits .....	125
Results and discussion.....	125
Assumptions in the model.....	125
Predictions of $\Phi_i$ and $\beta_i$ and $M_i$ .....	129
Biokinetic parameters and confidence limits .....	130
A new parameter: ratio of maintenance to maximum specific growth	
132	
Conclusions .....	134
5. CONCLUSIONS .....	135
REFERENCES CITED .....	138
APPENDICES.....	148
APPENDIX A: EFFECT OF BIOMINERALIZED MANGANESE ON PITTING	
CORROSION OF TYPE 304L STAINLESS STEEL.....	149
.....	
APPENDIX B: The MATLAB <sup>®</sup> code .....	172

## LIST OF TABLES

Table	Page
1.1. The composition of 316L stainless steel used in this study ( % w/w). .....	35
2.1. ATCC Culture Medium 1917 MSVP for <i>Leptothrix discophora</i> SP-6.....	57
2.2. Composition of 316L stainless steel.....	59
2.3. Passive film thicknesses in Angstrom for the coupons after removal of biofilm/-Mn-deposits.....	77
2.4. Pitting potentials of stainless steel coupons in 0.2 M NaCl. ....	82
3.1. ATCC Culture 1917 MSVP for <i>Leptothrix discophora</i> SP-6 (American Type Culture Collection Catalogue, 1992).....	91
3.2. Combined and single growth models were used to find the best model, and the corresponding biokinetic coefficients. ....	97
3.3. The data collected at various steady states. The chemostat was operated at temperature = 25°C, pH = 7.2, agitation rate = 350 rpm, $S_{FP} = 1000 \text{ mg L}^{-1}$ , $S_{fn} = 65 \text{ mg NH}_4^+ \text{ L}^{-1}$ .....	100
3.4. Growth models, biokinetic parameters, and SSD. First column shows the type of the model used in the simulation (See Equations 3.1-3.3). The third and fourth columns show the equations we combined to assemble the double substrate kinetic expressions. The results are presented in ascending order of SSD. K(p), column 7, refers to $K_{sMp}$ , $K_{sTp}$ , $K_{sMZp}$ and K(o), column 8, refers to $K_{sMo}$ , $K_{sTo}$ , $K_{sMZo}$ . ....	103
3.5. The models, which give the best SSD. The biokinetic parameters were calculated for actual data, and for simulated data sets.....	104
4. 1. Biokinetic parameters and confidence limits for biofilm and planktonic growth of <i>Leptothrix discophora</i> SP-6. Note the data for planktonic growth is exported from our previous study (Yurt et al., 2002). ....	131.

## LIST OF FIGURES

Figure	Page
1.1. Schematic representation of passive layers in the presence of water.....	5
1.2 Penetration mechanism for pit initiation .....	7
1.3 Adsorption mechanism for pit initiation. ....	8
1.4. Pit initiation by passive film breaking mechanism. ....	9
1.5. Manganese cycling at stainless steel surface hypothesized by Olesen et al., (2000). ....	13
1.6. Manganese cycling proposed by Shi et al., (2002). ....	14
1.7. The relation between pitting ( $E_{\text{pitting}}$ ) and corrosion ( $E_{\text{corr}}$ ) potentials for a clean metal. ....	16
1.8. Typical growth curve for a microbial growth. ....	18
1.9. Effects of substrate concentration on specific growth rate.....	20
1.10. An SEM picture of <i>Leptothrix discophora</i> SP-6 colony on stainless steel surface. ....	25
1.11. An SEM picture illustrating a single <i>Leptothrix discophora</i> SP-6.....	25
1.12. The progression of biofilm accumulation. ....	27
1.13. Polycarbonate coupon holder and accessories. ....	36
1.14. The reactor used to ennoblement experiments.....	38
1.15. A photograph of the reactor and data acquisition system. ....	39
1.16. The electrochemical cell used for anodic polarization consisted of three electrodes, a potentiometer, and a computer. ....	43
1.17. A typical anodic polarization curve. ....	44
1.18. Schematic diagram of chemostat used in this study.....	47

1.19. Diagram of a colony biofilm grown on top of a membrane filter. The growth substrate is supplied by the agar and transferred through the membrane to the biofilm. The microorganisms receive oxygen from the air .....	49
1.20. Schematic diagram of a Clark type dissolved oxygen sensor. The insert shows the position of the cathode, the reference electrode, and the silicone rubber membrane. ....	51
2.1. Depth profiles of O, C, Fe and Cr for the growth medium treated control coupon. ....	63
2.2. Depth profiles of O, C, Fe and Cr for the <i>L. discophora</i> biofilm treated control coupon following complete removal of biofilm. ....	64
2.3. Depth profiles of O, C, Fe and Cr for the ennobled coupon after removal of biomineral deposits. Notice that the passive layer thickness appears to remain the same as that of the control coupons. This is explained in terms of re-oxidation of the surface (see text). ....	23
2.4. Depth profiles of O, C, Fe and Cr for the <i>L. discophora</i> biofilm treated coupon without the removal of biofilms. ....	66
2.5. Depth profiles of O, C, Fe and Cr for the ennobled coupon without the removal of biofilms and biomineralized deposits. ....	67
2.6. XPS curve fit for the Fe $2_{p3/2}$ profile to determine the bulk and oxide contributions. ....	69
2.7. XPS curve fit for the Cr $2_{p3/2}$ profile to separate the oxide and bulk contributions. ....	69
2.8 a) Fe and Fe-oxides b) Cr and Cr-oxides depth profiles for growth medium treated coupon. ....	71
2.9 a) Fe and Fe-oxides b) Cr and Cr-oxides depth profiles for <i>L. discophora</i> biofilm treated coupon after removal of biofilms. ....	72
2.10 a) Fe and Fe-oxides b) Cr and Cr-oxides depth profiles for ennobled coupon after removal of biofilms and biomineralized deposits. ....	73
2.11 a) Fe and Fe-oxides b) Cr and Cr-oxides depth profiles for <i>L. discophora</i> biofilm treated coupons (without $Mn^{2+}$ ; no ennoblement) without removal of biofilm. ....	74
2.12 a) Fe and Fe-oxides b) Cr and Cr-oxides depth profiles for ennobled coupon without removal of the biomineral deposits. ....	75

2.13. ToFSIMS images of (a) $Mn^+$ , (b) $Cr^+$ and (c) $FeH^+$ for an ennobled coupon at 420-Angstrom depth.....	78
2.14. ToFSIMS images of (a) $Mn^+$ , (b) $Cr^+$ and (c) $FeH^+$ for an ennobled coupon at 2600-Angstrom depth.....	79
2.15. The variation of OCP by time. When an ennobled coupon was exposed to 0.2 M NaCl solution, the potential became unstable and then dropped sharply (after ~900 min) and remained more or less constant ~ -60 mV. The ennoblement potential was 364 mV <sub>SCE</sub> .....	81
2.16. The cyclic polarization curves of as received-polished coupon (a), biofilm treated coupon (b) and ennobled coupon (c) in 0.2 M NaCl. Scan rate is 5mV/sec.....	83
3.1. The specific growth rates, predicted from Equation 3.11 versus experimentally measured.....	105
3.2. $1/D$ versus $(S_{fp} - S_p)/X$ for pyruvate. The slope of the line gives $m_p$ and the intercept gives $1/Y_{X/P}$ .....	106
3.3. $1/D$ versus $SOUR/D$ . The slope of the line gives $m_o$ and the intercept gives $1/Y_{X/O}$ .....	107
4.1. A colony biofilm grown on the top of a membrane filter. The growth substrate is supplied by the agar, and is transferred through the polycarbonate membrane to the biofilm. The microorganisms receive oxygen from the air.....	115
4.2. The normalized dissolved oxygen concentration ( $S^*$ ) is plotted versus the normalized distance ( $x^*$ ) from the bottom in a colony biofilm of <i>Leptothrix discophora</i> SP-6.....	118
4.3. The algorithm we developed to compute biokinetic parameters in biofilms.....	123
4.4. Oxygen concentration profiles measured in 120 hours old colony biofilms grown on agar plates containing 1, 5, 10, 20 and 30 g/L pyruvate. When pyruvate concentrations exceeds 10 g/L, the oxygen profiles do not change much, indicating that pyruvate concentration is in excess and for these conditions the growth is limited by oxygen.....	126
4.5. Oxygen concentration profiles measured at different locations (1-5) in the colony biofilm. Location 1 was at the center of the microcolony and other locations were approximately 100 micrometers apart.....	127

4.6. Similar oxygen concentration profiles are measured in 120 and 144 hours old colony biofilms verify that oxygen consumption is at pseudo steady state. .... 129

## NOMENCLATURE

- $B_i$  Constant in Contois model for substrate  $i$  (mg substrate/mg microorganism)
- $D$  Dilution rate (1/h)
- $D_{eff}$  Effective diffusion coefficient of oxygen in biofilm ( $m^2/s$ )
- $i$  Subscript refers to the growth model, M for Monod and T for Tessier
- $K_{sM}$  Monod half rate coefficient ( $g/m^3$ )
- $K_{sMi}$  Monod half saturation constant for substrate  $i$
- $K_{sMZi}$  Moser constant for substrate  $i$
- $K_{sT}$  Tessier coefficient ( $g/m^3$ )
- $K_{sTi}$  Tessier saturation constant for substrate  $i$
- $L_f$  Biofilm thickness (m)
- $m$  maintenance coefficient for oxygen (mg microorganism/mg oxygen)
- $m_i$  Maintenance factor for limiting substrate  $i$ , (mg microorganism/mg substrate  $i$ )
- $m_M$  maintenance coefficient for oxygen when growth is described according to Monod kinetics (mg microorganism/mg oxygen)
- $m_T$  maintenance coefficient for oxygen when growth is described according to Tessier kinetics (mg microorganism/mg oxygen)
- $M_M = \frac{m_M L_f^2 X_f}{D_{eff} S_s}$

$$M_T = \frac{m_T L_f^2 X_f}{D_{eff} S_s}$$

- N Number of experiments (integer)
- Q Volumetric flow rate (L/h)
- S Oxygen concentration in biofilm ( $g/m^3$ )
- $S^*$  Dimensionless oxygen concentration in biofilm ( $=S/S_s$ )
- $S_{bottom}$  Oxygen concentration at the bottom of biofilm ( $g/m^3$ )
- $S^*_{bottom}$  Experimentally measured dimensionless oxygen concentration at the bottom of biofilm ( $=S_{bottom}/S_s$ )
- $S^*_{experimentally\_measured}$  Experimentally measured dimensionless oxygen concentration in the biofilm
- $S^*_{predicted}$  Calculated dimensionless oxygen concentration from the solution of the model in biofilm
- $S_{ei}$  Substrate concentration in effluent stream (mg/L)
- $S_{fi}$  Concentration of substrate  $i$  in influent stream (mg/L)
- $S_i$  Concentration of substrate  $i$  (mg/L)
- SOUR Specific oxygen uptake rate (mg oxygen/mg microorganism/h)
- $S_s$  Oxygen concentration at biofilm – air interface ( $g/m^3$ )
- SSD: Sum of squares of difference
- V Reactor volume (L)
- x Distance from the bottom of the biofilm (m)

- $X$  Microorganism concentration in chemostat (mg/L)
- $x^*$  Dimensionless distance from the bottom ( $=x/L_f$ )
- $X_f$  Biofilm density ( $\text{g/m}^3$ )
- $Y_{X/i}$  Yield coefficient for limiting substrate  $i$  (mg microorganism/mg limiting substrate)
- $Y_{x/o}$  Yield coefficient for oxygen (g microorganism produced/g oxygen consumed)

Greek letters

$$\beta_M = \frac{K_{sM}}{S_s}$$

$$\beta_T = \frac{K_{sT}}{S_s}$$

$\Phi$  Thiele modulus ( $\Phi_M$  or  $\Phi_T$ )

$$\Phi_M = \sqrt{\frac{\mu_{\max} L_f^2 X_f}{Y_{x/o} D_{\text{eff}} S_s}}$$

$$\Phi_T = \sqrt{\frac{\mu_{\max} L_f^2 X_f}{Y_{x/o} D_{\text{eff}} S_s}}$$

$\lambda_i$  Moser coefficient for substrate  $i$

$\mu$  Specific growth rate of microorganism, (1/h)

$\mu_{\text{experimental}}$  Experimentally determined specific growth rate of microorganism from  $(\mu=Q/V)$ , (1/h).

$\mu_i$  Specific growth rate of microorganism for limiting substrate  $i$ , (1/h)

$\mu_{\text{max}}$  Maximum specific growth rate ( $\text{s}^{-1}$ )

$\mu_{\text{model}}$  Specific growth rate of microorganism predicted from the models, (1/h)

### Subscripts

i Substrate

p Pyruvate

o Oxygen

n  $\text{NH}^{4+}$

## ABSTRACT

This thesis examined effects of manganese oxidizing bacteria, *Leptothrix discophora* SP-6 biofilms, on passive film chemistry and pitting corrosion of 316L stainless steel.

Biofilms of manganese oxidizing bacteria attach to the passive films of metals and deposit manganese oxides on the surfaces. These oxides, being in equilibrium with manganese ions in water, shift the corrosion potential of the passive metals in the noble direction, causing a phenomenon known as "ennoblement". Ennoblement is of interest because it increases corrosion potential, which may initiate localized forms of corrosion of passive metals, pitting corrosion. The mechanism of pit initiation on the ennobled coupons still is not completely known. For localized corrosion to occur, the passive film has to be broken down, and it has been speculated that the biofilms of manganese oxidizing bacteria have a direct effect on the chemistry of the passive films.

The effect of ennoblement of 316L stainless steel by biomineralized manganese deposits on chemistry of passive films was studied using surface-sensitive analytical techniques and cyclic polarization. Depth profiles of elements in the passive films on the ennobled coupons were analyzed using x-ray photoelectron spectroscopy (XPS), and distribution of metal elements were examined by time-of-flight secondary ion mass spectroscopy (ToFSIMS). The results showed that oxide layers on the ennobled coupons were thinner than those on the control coupons. Cyclic polarization curves showed that ennobled 316L stainless steel indicated significant loss of passivity. It was concluded that metabolic activity of manganese oxidizing bacteria, *Leptothrix discophora* SP-6 degraded the quality of the passive film on stainless steel coupons by locally reducing its thickness and lowering the pitting potential.

To relate the kinetics of ennoblement to the rate of deposition of manganese oxides on metal surfaces, growth kinetics of *Leptothrix discophora* SP-6 were quantified in biofilms and in planktonic form. In planktonic form, double-substrate growth kinetics, using Monod growth kinetics for pyruvate and Tessier growth kinetics for oxygen, showed the best agreement with the experimental data. Monod model of microbial growth kinetics adequately represents the growth of *Leptothrix discophora* SP-6 biofilms.

## CHAPTER 1

## INTRODUCTION

This thesis examines several effects of growth and attachment of *Leptothrix discophora* SP-6 in biofilms. The effects of biofilms of these manganese oxidizing bacteria on passive film chemistry and on the pitting potentials of 316L stainless steel were investigated. Also, the growth kinetics of *Leptothrix discophora* SP-6 were determined for planktonic and biofilm growth. This introductory section briefly describes the content of the thesis, presents research questions and hypotheses to be addressed, and shows the organization of the thesis.

A research group at the Montana State University (MSU) is systematically studying the ennoblement of stainless steel by microbially deposited manganese oxides. It has been shown that biofilms of *Leptothrix discophora* SP-6 grown on 316L stainless steel (SS) increase the open circuit potential to values of 300 – 400 mV<sub>SCE</sub> by depositing manganese oxides (Olesen et al., 2000a,b; Dickinson et al., 1996). This phenomenon, which increases the open circuit potential, is called ennoblement. The manganese deposition mechanism and ennoblement on stainless steel coupons have been well described by the MSU research group (Shi et al., 2002; Olesen et al., 2000a,b; Dickinson et al., 1996). The ennoblement increases risk of pitting corrosion by lowering pitting potential of stainless steel in the presence of

active ions such as chloride (Olesen et al., 2001; Amaya and Miyuki 1997; Linhardt 1996; Suleiman et al., 1994). One of the possible mechanisms that could lower pitting potential is that the passive film is degraded by ennoblement caused by manganese deposition. Continuing the efforts at MSU, the first part of this thesis investigates passive film chemistry, explores these processes, presents previous literature and states research goals (section 1.1). The research correlating passive film chemistry and pitting potential of stainless steel ennobled by biomineralized manganese was prepared as a research paper and is presented in chapter 2 (Yurt et al., 2002a). The effect of biomineralized manganese on pitting corrosion of type 304L stainless steel are examined, and the basic approach to measure pitting corrosion of stainless steel 304L used in this thesis, and tests results of pitting potentials for clean and ennobled coupons, are presented in the appendix as a published paper (Olesen, B. H., Yurt, N., Lewandowski, Z. 2001).

For ennoblement studies, the model microorganism used at MSU has been *Leptothrix discophora* SP-6, which grows in bulk liquid, attaches to stainless steel surfaces, grows as biofilms and then deposits manganese and causes ennoblement. The second part of this thesis explores quantification of the growth kinetics of *Leptothrix discophora* SP-6 in planktonic and biofilm forms. Discussion of microorganism growth in planktonic form and in biofilms along with a literature review and research goals are presented in section 1.3. The growth kinetics of *Leptothrix discophora* SP-6 in planktonic form is presented as a research paper in chapter 3 (Yurt et al., 2002b). Since there was not any adequate published method to

calculate biokinetic parameters in biofilms, I developed an algorithm to extract biokinetic parameters of microorganism growth in *Leptothrix discophora* SP-6 biofilms. The developed algorithm and biokinetic parameters for *Leptothrix discophora* SP-6 biofilms are presented as a research paper in chapter 4 (Yurt et al., 2002c). The developed algorithms to calculate biokinetic parameters for planktonic growth and biofilm growth are integrated into MATLAB programs. These MATLAB programs were added to corresponding sections as an appendix to make them available for other researchers, since they are not available in the literature.

The experimental methods and instruments used in the thesis are presented in section 1.4 for future reference.

The hypotheses addressed in this thesis are:

1. Manganese oxidizing activity of *Leptothrix discophora* SP-6 in a biofilm leads to ennoblement of stainless steel and causes changes in the passive film chemistry of the steel.
2. The presence of biomineralized manganese oxides on the surface of 316L stainless steel initiates pitting corrosion in a low-chloride aqueous environment.
3. The statistically optimum model to represent *Leptothrix discophora* SP-6 growth in the planktonic form can be determined by an algorithm, developed by the author, which optimizes parameters for the four major kinetic models.

4. The statistically optimum model to represent *Leptothrix discophora* SP-6 growth in the biofilm form can be determined by an algorithm, developed by the author, which optimizes parameters.
5. *Leptothrix discophora* SP-6 has different growth and substrate consumption kinetics in planktonic and biofilm form.

Surface sensitive techniques such as XPS, ToFSIMS were used to determine passive film chemistry and thickness. The anodic polarization technique was used to measure pitting potentials. Hypotheses 1 and 2 are addressed in chapter 2. A chemostat operated at steady state was used to determine the best growth model, along with corresponding biokinetic parameters of *Leptothrix discophora* SP-6, and hypothesis 3 is addressed in chapter 3. Dissolved oxygen microsensors were used to measure concentration profiles in *Leptothrix discophora* SP-6 biofilms. A new method was developed to extract the best representative growth model and corresponding biokinetic parameters of *Leptothrix discophora* SP-6 growth in biofilms. Hypotheses 4 and 5 are addressed in chapter 4. Chapters 2, 3, and 4 are presented in the format of a journal paper.

### Manganese Biomineralization on 316L Stainless Steel

#### Stainless Steels

Stainless steels are iron-chromium alloys with a minimum of 10 wt % chromium. When the steel contains at least that much chromium, a thin, transparent,

protective passive film forms on the surface. The passive film forms spontaneously as a result of the reaction between the chromium in the steel and the oxygen in the air. The passive film is a barrier between the steel and the environment and prevents corrosive attack of the underlying steel as long as the passive film remains intact. This protective passive film is quite thin, on the order of nanometers, and its actual composition depends on the alloying elements in the stainless steel and the environment to which it is exposed (Figure 1.1).

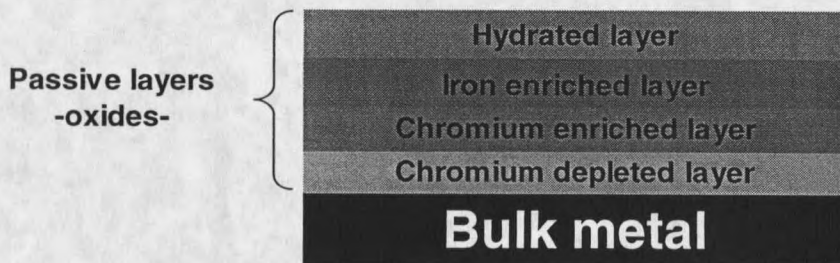


Figure 1.1. Schematic representation of passive layers in the presence of water.

### Pitting Corrosion

Pitting is localized attack at a point where the passive film can no longer protect the stainless steel. Theoretically, pitting processes consist of the following stages; 1) passive film breakdown, 2) metastable pit formation, and 3) pit growth. These stages are discussed below.

Passive Film Breakdown. The breakdown of the passive film is the initiation of the pitting process. The breakdown happens rapidly on a very small scale, which

makes direct observation difficult. The passive film can be drawn schematically as a simple inert layer covering the underlying metal, blocking access of the environment to the metal (see Figure 1.2). Depending on alloy composition, environment, potential, and exposure history, this film can have a range of thickness, structure, composition, and protectiveness. Typical passive films are quite thin, and support an extremely high electric field (on the order of  $10^6$ - $10^7$  V/cm). The passage of a finite passive current density is evidence of continual reaction of the metal, with resultant film thickening, dissolution into the environment, or some combination of the two. The view of the passive film as a *dynamic structure*, rather than static, is critical to the proposed mechanisms of passive film breakdown and pit initiation.

Theoretically, passive film breakdown and pit initiation have been categorized according to three main mechanisms; 1) passive film penetration, 2) film breaking and, 3) adsorption.

Figure 1.2 shows the penetration mechanism for pit initiation. It involves the transport of the aggressive anions through the passive film to the metal/oxide interface where accelerated dissolution of metal is promoted (Hoar 1965).

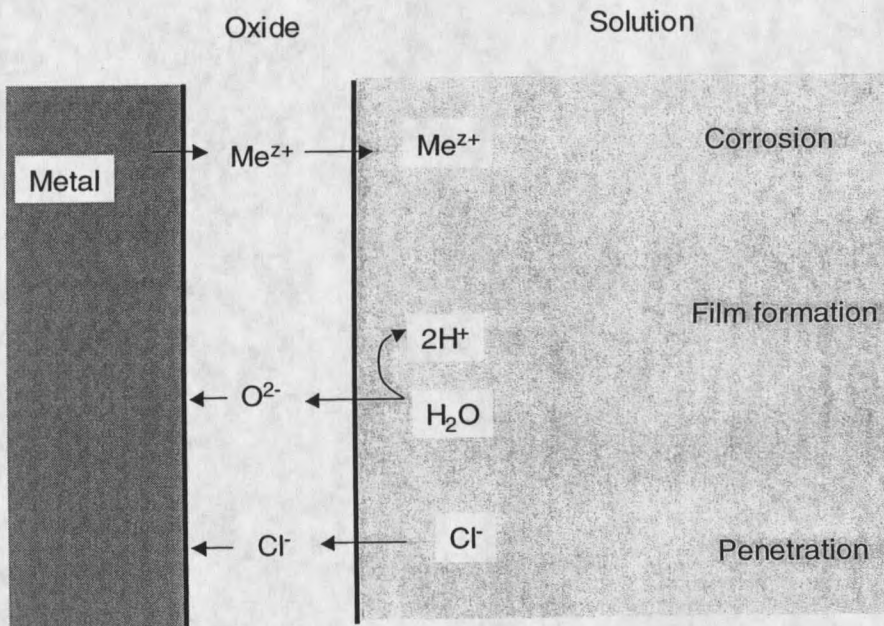


Figure 1.2 Penetration mechanism for pit initiation.

The adsorption model is presented schematically in Figure 1.3. Localized adsorption of chloride ion leads to an enhanced oxide dissolution at the sites with subsequent thinning of the oxide film until, finally, a complete removal is achieved and active metal dissolution starts. Basically adsorbed chloride ions compete with oxygen, chromates, or any other passivating agent for a place on the metal surface (Uhling 1950). However, the chloride ions do not remain adsorbed because the metal – halogen reaction rate is high (Uhling 1950). The metal, therefore, is rapidly attacked at restricted areas where chlorides succeed in displacing the adsorbed passivator and passivity breaks down. This theory was originally proposed by Uhling (1950). However, based on XPS measurements later on it has been shown that exposure of Fe to chloride and other halides caused thinning of the passive film, even

under conditions where a pit had not formed (Strehblow 1995). This contradicted Uhling's adsorption theory. However, this can be explained according to Hoar's theory for chloride adsorption: when thinning occurs locally because of some local adsorbed species, the local electric field strength will increase, which may eventually lead to complete breakdown and the formation of a pit (Hoar 1965).

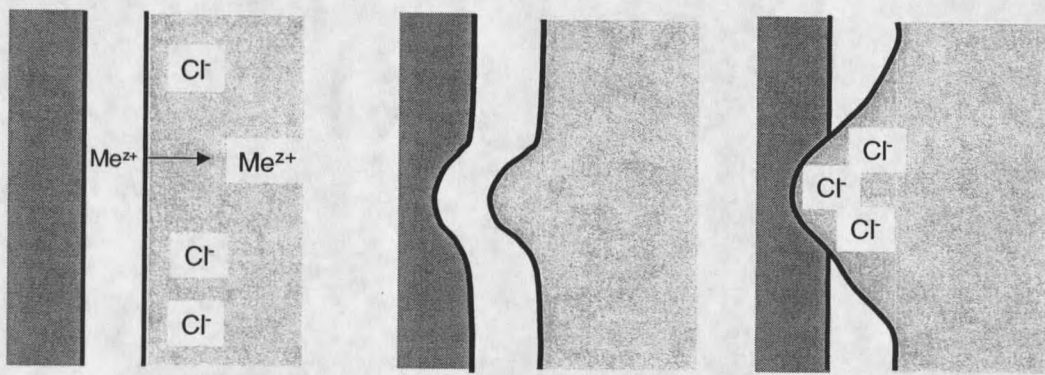


Figure 1.3 Adsorption mechanism for pit initiation.

Figure 1.4 shows pit initiation by the passive film breaking mechanism. This approach assumes that the thin passive film is in a continual state of breakdown and repair (Richardson and Wood 1970). Mechanical stresses at weak sites or flaws may cause the local breakdown events, which rapidly heal in non-aggressive environments. In fact, the background passive current density may be derived from a summation of many such breakdown and repair events (Kruger 2000). In chloride-containing solutions, however, there would be a lower likelihood for such a breakdown to heal because of the inhibition of repassivation by chloride. The passive film-breaking model really involves initiation based on pit growth stability. It

assumes that passive film breakdown will always occur, although at a rate that depends on many factors related to the passive film properties. According to this model, common and frequent breakdown will only lead to pitting under conditions where pit growth is possible (Bohni 2000). If, as stated by the passive film-breaking theory, passive film breakdown is frequent and rapid, pit initiation depends on generation of the conditions needed for a pit to be able to grow.

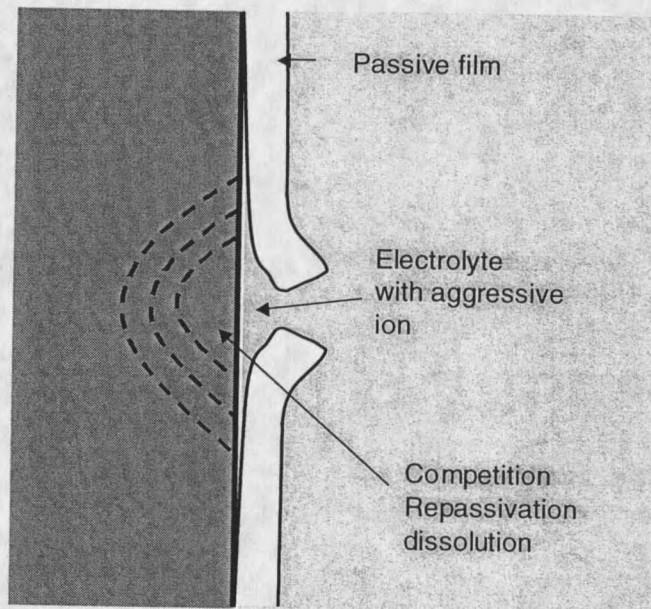


Figure 1.4. Pit initiation by passive film breaking mechanism.

Metastable Pitting. Pits which initiate and grow for a limited period before repassivating are called metastable (Bohni 2000). Large pits can stop growing for a variety of reasons, but metastable pits are typically considered to be only  $\mu\text{m}$  size at most with a lifetime on the order of seconds or less. Metastable pits can form at potentials far below the pitting potential (which is associated with the initiation of

stable pits). It has been shown that when stable pits are small, they behave identically to metastable pits (they open and close). Stable pits survive the metastable stage and continue to grow, whereas metastable pits repassivate and stop growing for some reason.

Pit Growth. Pit growth depends on material composition, pit electrolyte concentration and pit-bottom potential. The mass-transport characteristics of the pit influence pit growth kinetics through the pit electrolyte concentration. Pit stability depends upon the maintenance of pit electrolyte composition and pit bottom potential that are at least severe enough to prevent repassivation of the dissolving metal surface at the pit bottom. Pit growth can be controlled by the same factors that can limit any electrochemical reaction (Bohni 2000).

At the end of pit growth process, the metal corrodes and fails. Generally stainless steel considered as a metal immune to pitting. As described in the following section, recently it has been shown that stainless steel pits when microorganisms are grown at the surface and deposit minerals.

#### Manganese Biomineralization and Manganese Cycle

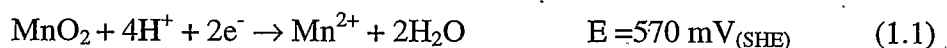
Biofilms have been reported to modify surface chemistry and electrochemistry of metals in natural waters. An example of such modification is ennoblement of passive metals. During ennoblement process, open circuit potential (OCP) of microbially colonized metal elevates from -200 mV to 350 mV SCE with an associated increase in cathodic current. This shift of OCP is called as *ennoblement*.

Mollica and Trevis (1988) were the first to report an observed increase in the open circuit potential of passive metals when immersed in natural waters. Dexter and Gao (1988) reported similar ennoblement effects from 316L exposed marine biofilm. Scotto et al., (1985) reported an increase in OCP of 22Cr3Mo0.6Ti steel up to 375 mV during 65 days of seawater exposure. Motoda et al., (1990) reported OCP values of 400 mV<sub>SCE</sub> over 10 days of seawater exposure for 18 different type of stainless steels, and titanium reached 350 mV<sub>SCE</sub> during the same period of time exposure. Eashwar et al., (1995) exposed titanium to seawater and changed illumination intensity from dark to strong intensity. The samples with moderate illumination only showed ennoblement. Numerous other studies have shown similar observation of passive metal ennoblement (Holthe et al., 1988 ; Little et al., 1990; Eashwar and Maruthamuthu 1995).

A variety of hypotheses were offered to explain the mechanisms of this ennoblement: 1) Depolarization of the oxygen reduction reaction caused by enzymes (Scotto and Lai 1998; Mollica et al., 1990; Scotto et al., 1985) or by iron chelators (siderophores) (Eashwar et al, 1995), 2) strong acidification of electrode surfaces due to biofilm activity (Little et al., 1991) and 3) combination of elevated H<sub>2</sub>O<sub>2</sub> concentration and decreased pH (Chandrasekaran et al., 1993). Although all researchers show that ennoblement is linked to biofilm formation, none of these hypotheses has been proven either in the laboratory or in the field.

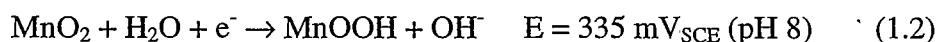
Linhardt (1996) observed a connection between microbial deposition of manganese and ennoblement of passive metals. He reported pitting corrosion of turbine runner blades (CrNi134) in a hydroelectric power plant in the Netherlands by

activity of manganese oxidizing microorganisms. SEM/EDAX and X-ray diffraction analysis of deposits on turbine blades showed significant amounts of manganese oxyhydroxide and manganese dioxide. Some of the deposits from the turbine blades were pressed into a pellet and then connected to a hydrogen reference electrode to measure the potential. A potential of 570 mV was measured. Linhardt concluded that the presence of manganese dioxide on the surface was responsible for the increase of the corrosion potential by the reaction:



This elevated potential caused pitting corrosion at a very low chloride concentration (20-170 mg/L), which normally is not enough to cause pitting itself.

In the Center for Biofilm Engineering, Dickinson et al., (1996) exposed stainless steel coupons in fresh river water and observed an increase in OCP from – 150 mV to 350 mV and 2-3 fold increase in cathodic density over 35 days. Epifluorescence and scanning electron microscopy of coupon surfaces detected Mn-rich annular deposits, associated clusters of bacterial cells, and abundant sheeted bacteria. Dickinson et al., (1996) demonstrated the same increase in potential and cathodic density by coating stainless steel surface by  $\text{MnO}_2$  paste and concluded that the observed electrochemical changes on stainless steel were caused by microbial deposition of manganese oxides. The following reaction is proposed for ennoblement:



After Dickinson, Olesen et al., (2000a) identified types of manganese oxides deposited by pure bacteria on 316L SS coupons using X-rays photoelectron spectroscopy. To show the kinetics of reduction of manganese oxides, electroplated

manganese oxide on a steel surface was reduced electrochemically. According to XPS analysis before and after electrochemical reduction, manganese oxide reduced to divalent manganese,  $\text{Mn}^{2+}$ , obtaining 2 electrons from the anodic corrosion sites.  $\text{MnOOH}$  was determined as an intermediate product in this section. Olesen et al., (2000a) suggested the manganese cycling on stainless steel shown in Figure 1.5.

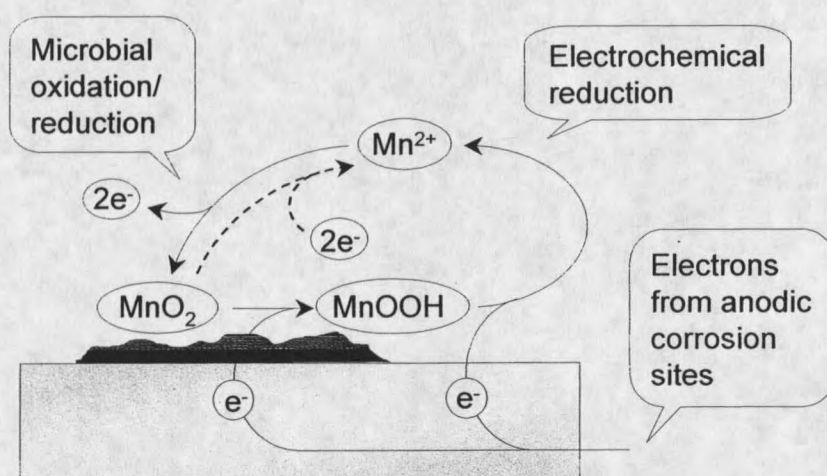


Figure 1.5. Manganese cycling at stainless steel surface hypothesized by Olesen et al., (2000).

Two years after Olesen (2000a), Shi et al., (2002), from the Center for Biofilm Engineering, improved the knowledge of the manganese cycle. They applied time of flight secondary ion mass spectroscopy to identify manganese oxides deposited by *Leptothrix discophora* SP-6. Their results indicated that the  $\text{Mn}^{2+}$  is oxidized microbiologically to  $\text{MnOOH}$ ; then  $\text{MnOOH}$  is further oxidized to  $\text{MnO}_2$ . They schematically represented their hypothesis on the manganese cycle in Figure 1.6.

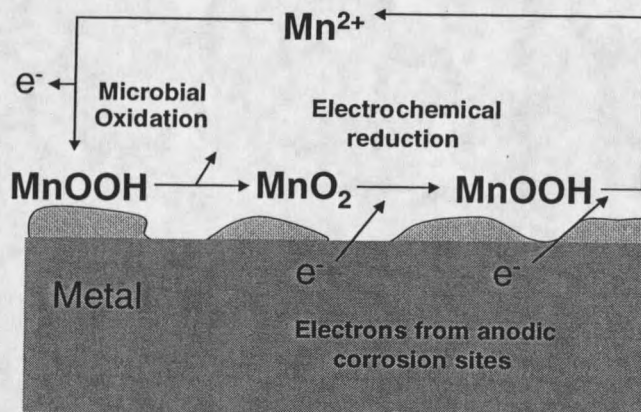


Figure 1.6. Manganese cycling proposed by Shi et al., (2002).

### Role of Passive Film Layer During Manganese Biomineralization on Stainless Steel Surface

As explained above, the passive film is a protective oxide layer on the stainless steel surface. When biofilms attach on stainless steel surfaces and start to deposit minerals, they cause development of anodic and cathodic sites on stainless steel surface due to biofilm heterogeneity, as claimed by George et al., (2000). Although, George et al., (2000) found cathodic and anodic sites on surface, these sites might be not only biofilm heterogeneity, but as a result of biomineralization i.e., the manganese cycle. In another study, Maruthamuthu et al., (1996) employed electrochemical techniques to measure passive film layer chemistry with an intact biofilm. They suggested that the mechanism of ennoblement is linked to the bacterial removal of excess anions and cations from the oxide film.

Hypothesis 1. Manganese oxidizing activity of *Leptothrix discophora* SP-6 in a biofilm leads to ennoblement of stainless steel and causes changes in the passive film chemistry of the steel.

To test this hypothesis, it is required to probe chemistry of the passive films on stainless steel coupons with intact biofilms. Pendyala (1996) studied chemical effects of biofilm colonization on stainless steel. She grew a mixed culture *Pseudomonas aeruginosa*, *Pseudomonas fluorescens* and *Klebsiella pneumoniae* and quantified passive film thickness on stainless steel sample with intact biofilms. Although her coupons were not ennobled, her study showed the possibility of measurement of passive film thickness on stainless steel coupons with an intact biofilm. Beech and Gaylarde (1999) explored how XPS can be used to quantify passive film chemistry at metal surfaces. From the same group Beech et al., (2000 a, b) later used XPS to quantify passive film chemistry of stainless steel coupons in the presence of *Pseudomonas* NCIMB2021. The method developed by Pendyala (1996) was used to measure passive film layer thicknesses to address hypothesis 1. The results of passive film thickness measurements are presented in Chapter 2.

Hypothesis 2. As stated before, biomineralization on stainless steel surface increases risk of the failure of the stainless steel. 316L stainless steel was expected to be immune to pitting in natural water, as demonstrated by Szklarsaka (1986) even at high chloride concentrations. However, there is experimental evidence that ennobled 316L stainless steel pits even at low chloride concentration (Amaya and Miyuki 1997; Suleiman et al., 1994; Felder 1994; Kobrin 1976). In another study, Neville and

Hodgkiess (2000) correlated passive film constitution with corrosion resistance; a thicker passive film makes stainless steel more corrosive resistant. If biomineralization of manganese on stainless steel coupons compromises passive film quality, stainless steel must pit at low chloride concentration. My second research hypothesis is;

*The presence of biomineralized manganese oxides on the surface of 316L stainless steel initiates pitting corrosion in a low-chloride aqueous environment.*

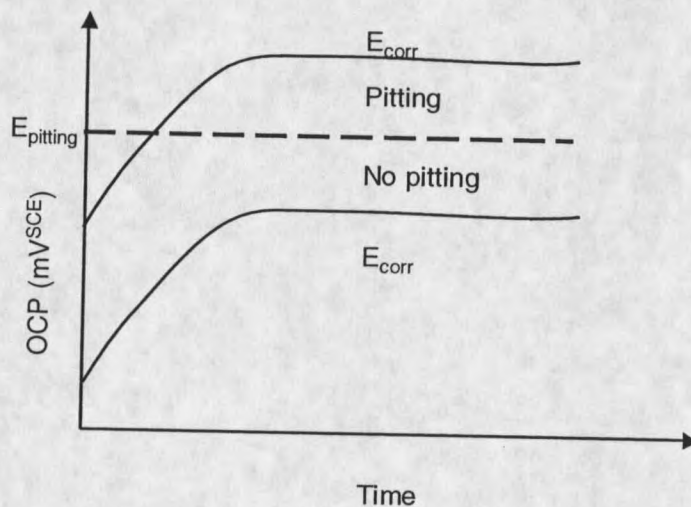


Figure 1.7. The relation between pitting ( $E_{\text{pitting}}$ ) and corrosion ( $E_{\text{corr}}$ ) potentials for a clean metal.

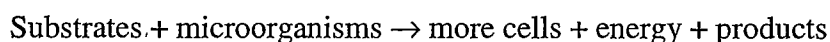
The relation between pitting ( $E_{\text{pitting}}$ ) and corrosion ( $E_{\text{corr}}$ ) potentials for a clean metal is presented in Figure 1.7. When corrosion potential of an ennobled metal is above the pitting potential, there is a possibility of pitting (Sedrix 1996). However, if corrosion potential of an ennobled metal is below the pitting potential, pitting does

not occur. To address my second research hypothesis given above, it is required to measure pitting potentials of clean and ennobled coupons. I developed anodic polarization techniques and tested coupons of 304L stainless steel (Olesen B. H., Yurt, N., Lewandowski, Z. 2001). It was found that ennoblement lowers pitting corrosion in a chlorinated environment for 304L stainless steel coupons. This study is presented in Appendix A. The same measurement techniques were utilized by Olesen B. H., Yurt, N., Lewandowski, Z. (2001) to measure corrosion potentials of ennobled 316L stainless steel coupons and the results are presented in Chapter 2.

### Biokinetics of Microbial Growth

#### Microbial Growth

For microorganisms, growth is an essential response to their physiochemical environment. Microbial growth is defined as an increase in cell numbers (by replication) and changes in cell size (Shuler and Kargi, 1992). Microorganisms use substrates and in a suitable medium, temperature and pH, convert them into biological compounds. The substrates are used for microorganism growth, energy production and product formation. Simply, this process can be described by the following equation.



(1.3)

The term “substrate” is used to describe a chemical (or nutrient) which is used by the microorganisms (e.g glucose, oxygen, pyruvate, etc).

The microbial growth is characterized by the *specific growth rate* ( $\mu$ ), which is defined as

$$\mu = \frac{1}{X} \frac{dX}{dt} \quad (1.4)$$

Here  $X$  is the dry weight microorganism concentration, usually (g/L),  $t$  is time, (h), and  $\mu$  is the specific growth rate, ( $\text{h}^{-1}$ ). As engineers, when we use the term “rate” we expect to see variation of a quantity by unit time. However, the specific growth rate is described as the normalized growth rate by dividing the microbial growth rate ( $dX/dt$ ) by the microorganism concentration, as given in Equation 1.4. A typical growth curve showing the correlation between microorganism concentration and time for a batch growth is presented in Figure 1.8.

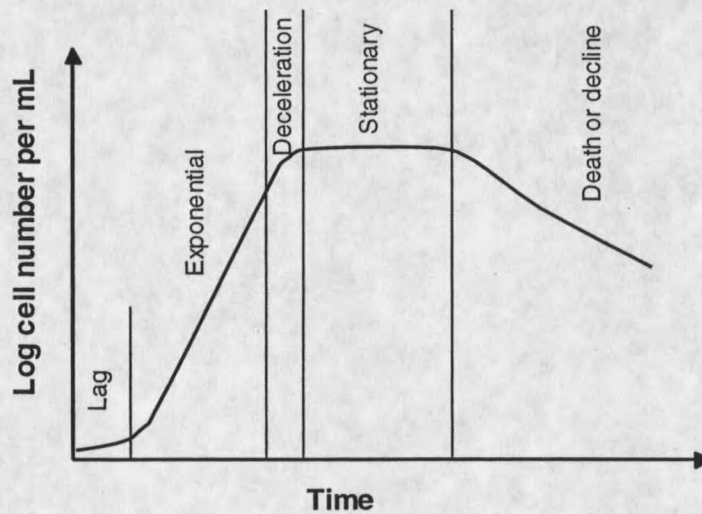


Figure 1.8. Typical growth curve for a microbial growth.

When a liquid medium is inoculated with a seed microorganism (inocula), the microorganism uses substrate in the medium and increases cell numbers as shown in Figure 1.8. The growth consists of five different phases; 1) the *lag phase* occurs immediately after inoculation and it is the time required for the adaptation of the cells to the new environment, 2) the *exponential growth phase*, also known as the logarithmic growth phase, occurs when, the microorganism concentration, or numbers, increase exponentially and the specific growth rate is described by equation 1.4, 3) the *deceleration phase* follows the exponential phase and the growth decelerates due to depletion of one or more essential substrates or accumulation of toxic microbial products, 4) the *stationary phase* starts at the end of deceleration phase, when the net growth rate is equal to zero, 5) the *death phase* (or decline phase) follows the stationary phase and in this phase total microorganism concentration decreases.

### Microbial Growth Kinetics

Microbial growth kinetics is the relationship between specific growth rate ( $\mu$ ) of a microorganism and the substrate concentration (S). It is a basic tool used to describe microbial growth and was established in the 1940s and 1950s with the key publications by Hinshelwood (1946), Monod (1949 and 1950), van Niel (1949), Novick and Szilard (1950), Herbert et al., (1956), Málek (1958), Pirt (1965). In these early papers, Monod (1949 and 1950) presented a model describing his experimental data and correlated specific growth rate with growth limiting substrate

concentration. A sample figure correlating growth limiting substrate concentration to specific growth rate is presented in Figure 1.9.

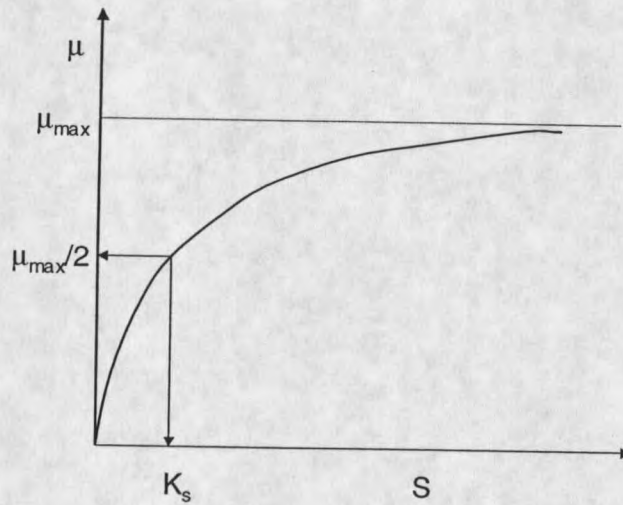


Figure 1.9. Effects of substrate concentration on specific growth rate.

As an example growth model, the Monod model is selected and discussed in the following sections (Monod 1949 and 1950). According to Monod and as seen from Figure 1.9, the specific growth rate is described as a function of substrate concentration given by the following equation.

$$\mu = \mu_{\max} \frac{S}{K_{SM} + S} \quad (1.5)$$

Two constants are used to describe the growth rate; (1)  $\mu_{\max}$  is the maximum growth rate when the substrate concentration is no longer limiting, [ $\text{time}^{-1}$ ].  $K_s$  is the Monod half saturation constant, [mass (or moles) per unit volume].  $K_s$  is equal to substrate concentration when  $\mu = \mu_{\max}/2$ .

Note, that the Monod growth kinetic model given above is valid only when microbial growth is limited by a single substrate. For many years the Monod equation was recognized as “fundamentally true” and some microbiologist considered it one of the major laws, such as Newton’s mechanics, Coulomb’s laws of electricity, etc. In the 1950s, there were a few studies devoted to testing the Monod equation (Moser 1958; Contois 1959). These authors found that not all experimental data could be reasonably well fitted by Monod’s equation. A better fit could be obtained by using the following, entirely empirical, equations.

$$\text{Moser} \quad \mu = \mu_{\max} (1 + K_{sMZi} S^{-\lambda_i})^{-1} \quad (\text{Moser, 1958}) \quad (1.6)$$

$$\text{Contois} \quad \mu = \mu_{\max} \frac{S_i}{B_i X + S_i} \quad (\text{Contois, 1959}) \quad (1.7)$$

Another model used in the literature was developed by Tessier (1942) by hypothesizing that the dependence of specific growth rate on the substrate concentration was proportional to the difference between  $\mu$  and  $\mu_{\max}$ :

$$\frac{d\mu}{dS_i} = \frac{1}{K_{sT}} (\mu_{\max} - \mu) \quad (1.8)$$

Equation 1.8, when integrated, gives the well-known form of the Tessier Equation (Equation 1.9).

$$\text{Tessier} \quad \mu = \mu_{\max} (1 - e^{-S_i/K_{sT}}) \quad (\text{Tessier, 1942}) \quad (1.9)$$

Equations 1.5, 1.6, 1.7, and 1.9 are general growth kinetics equations to describe single substrate limited growth. Since for the present study I am interested

only in saturation type of kinetics, I did not include any inhibition type of growth kinetics.

### Multiple Substrate Limited Growth

When microbial growth is limited by more than one substrate, three forms of multiple substrate growth kinetics can be considered (Bailey and Ollis 1986; Shuler and Kargi 1992):

(1) An interactive or multiplicative form,

$$\mu/\mu_{\max} = [\mu(S_1)] [\mu(S_2)] \dots \dots [\mu(S_i)] \quad (1.10)$$

(2) An additive form,

$$\mu/\mu_{\max} = [\mu(S_1) + \mu(S_2) + \dots \dots + \mu(S_i)]/i \quad (1.11)$$

(3) A non interactive form,

$$\mu/\mu_{\max} = \min [\mu(S_1) \text{ or } \mu(S_2) \text{ or } \dots \dots \text{ or } \mu(S_i)] \quad (1.12)$$

### Substrate Utilization Rate

Substrate utilization rate in a batch chemostat is described as the variation of substrate concentration by time and it is given by Equation 1.13.

$$-\frac{dS}{dt} = \frac{1}{Y_{x/s}} \frac{dX}{dt} \quad (1.13)$$

Equation 1.13 was originally recommended by Monod (1949 and 1950); later Powell (1967) and Pirt (1965) added a maintenance term (Equation 1.14) to define substrate consumption rate because Equation 1.13 could not represent their experimental data:

$$-\frac{dS}{dt} = \frac{1}{Y_{x/s}} \frac{dX}{dt} + mX \quad (1.14)$$

### Determination of Microbial Growth Kinetics

Microbial growth kinetic parameters are usually determined using a chemostat (Shuler and Kargi 1992) operated at batch or at steady state. Batch systems generally are not preferred because of difficulty in determining correct substrate concentration and specific growth rates. By operating a chemostat at steady state and at different dilution rates, one can calculate biokinetic parameters as described in Chapter 3. This is the correct and best way of determining growth kinetics; however, it requires considerable time and effort (Panikov 1995). In a chemostat operated at steady state, the specific growth rate is considered as an independent variable and it is equal to the dilution rate,  $D$ , as given by Equation 1.15.

$$\mu = D = Q/V \quad (1.15)$$

The term “growth kinetics” is used to refer any of the growth models described by Equations 1.5, 1.6, 1.7 and 1.9, and the term “biokinetic parameters” is used to refer the constants in these equations. I also used the term “biokinetic parameters” to describe a group of constants used to describe microbial growth and substrate utilization as presented in chapter 4.

*Leptothrix discophora* SP-6

*Leptothrix discophora* SP-6 is a member of the *Sphaerotilus Leptothrix* group, which are manganese and iron oxidizing sheathed bacteria that thrive in iron- and manganese-rich environments such as iron seeps, swamps, and springs (Emerson and Ghiorse, 1992). Although *Leptothrix discophora* is not a pathogen, it is considered a nuisance in water distribution systems because it oxidizes iron and manganese, causes color problems, and in extreme cases clog water distribution conduits. In the Center for Biofilm Engineering, the metabolic activity of biofilms of manganese oxidizing bacteria, *Leptothrix discophora* SP-6 and their effect on microbially influenced corrosion (MIC), specifically on pitting corrosion of stainless steels, have been extensively studied (Dickinson and Lewandowski, 1996; Dickinson et al., 1996; Olesen et al., 2000a,b). For that reason, I used *Leptothrix discophora* SP-6 as a model microorganism in my thesis. Figure 1.10 shows an SEM picture of *Leptothrix discophora* SP-6 colony on a stainless steel surface. Similarly, Figure 1.11 illustrates a single *Leptothrix discophora* SP-6 on a stainless steel surface.

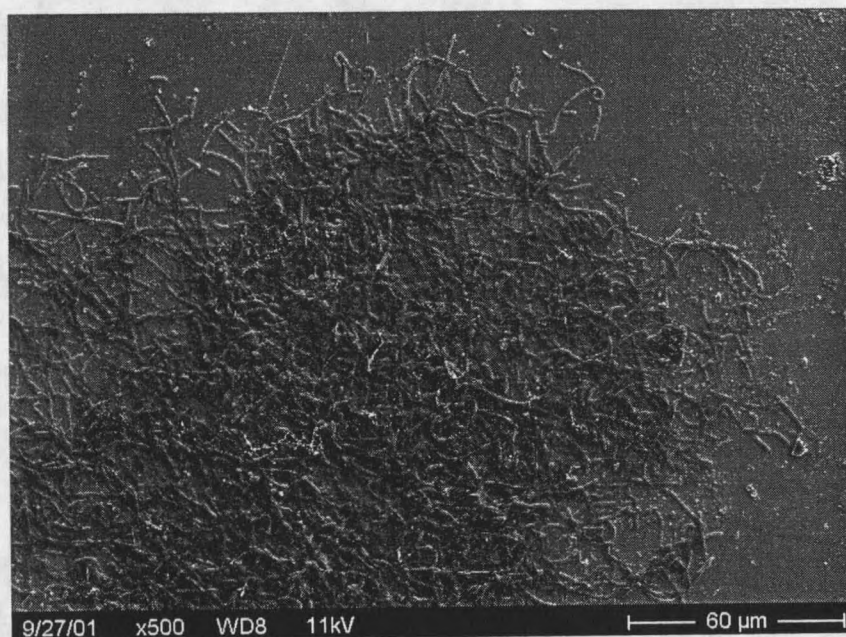


Figure 1.10. An SEM picture of *Leptothrix discophora* SP-6 colony on stainless steel surface.

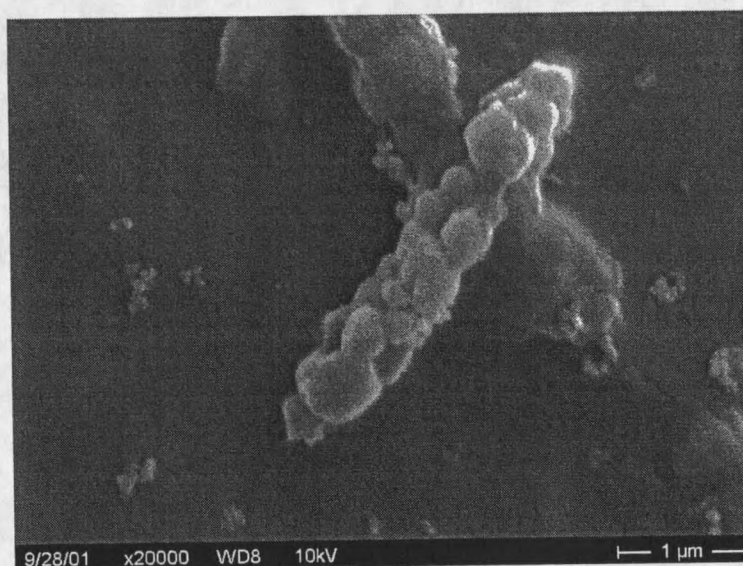


Figure 1.11. An SEM picture illustrating a single *Leptothrix discophora* SP-6.

### Growth Kinetics of *Leptothrix discophora* SP-6

To construct mathematical models of microbially induced corrosion caused by manganese oxidizing bacteria it is important to evaluate two factors: (1) growth kinetics of the microorganisms involved and (2) rate of manganese oxide deposition in biofilms deposited on metal surfaces. However, studying all these factors was difficult. For that reason, I focused on the first factor and studied the growth kinetics of *Leptothrix discophora* SP-6 with the following hypothesis.

Hypothesis 3. *The statistically optimum model to represent Leptothrix discophora SP-6 growth in the planktonic form can be determined by an algorithm, developed by the author, which optimizes parameters for the four major kinetic models.*

To address hypothesis 3, my specific goals were 1) operate a chemostat at steady state and measure substrate and microorganism concentrations, 2) test equations 1.5, 1.6, 1.7 and 1.9 in representing experimental data, 3) find the best representative equation, 4) calculate biokinetic parameters, along with standard deviations, using Monte Carlo simulations.

### Biofilm Growth

Microbial growth in biofilms is similar to microbial growth for planktonic microorganisms. However, generally attached cell number per unit surface area, on

attached biomass or surface coverage of biomass, are used to describe biofilm growth.

The progression of biofilm accumulation is schematically presented in Figure 1.12.

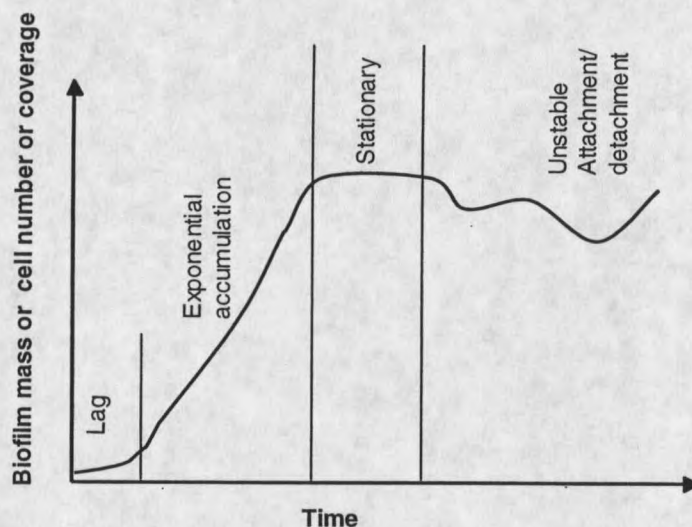


Figure 1.12. The progression of biofilm accumulation.

When a biofilm reactor such as a flat plate flow cell (Lewandowski et al., 1999) is inoculated with a seed microorganism (inocula), microorganisms attach to the reactor surfaces. The *lag phase* occurs immediately after attachment. During this time microorganisms adapt to the surface. The *exponential accumulation phase* is also known as logarithmic growth phase. In this phase, the microorganisms on the surface grow exponentially and increase cell number or total biomass or surface coverage. The *stationary phase* starts at the end of exponential accumulation phase. In this phase the biofilm thickness or total biomass or total number of cells reaches to a constant value. The *unstable phase* follows the stationary phase and in this phase,

there are detachments from the biofilm, attachments to the biofilm and biofilm growth.

The biofilm growth up to stationary phase was experimentally examined by Lewandowski et al., (1999), and later the reproducibility of biofilm growth up to the stationary phase was experimentally presented by Jackson et al., (2001).

### Microbial Growth in Biofilms

The microbial growth in biofilms is described using exactly the same growth models used for planktonic microorganisms. Biokinetic parameters for different microorganisms and substrate are well studied and presented in the literature for planktonic growth (see previous section). Most authors have used biokinetic parameters obtained from planktonic culture experiments to describe microbial growth in biofilms (Kreft and Wimpenny 2001; Eberl et al., 2000; Noguera et al., 1999; Beyenal et al., 1997; Bakke et al., 1989). Because the physiology and species composition of biofilm systems are expected to be different than suspended growth systems, it is not proven that biokinetic parameters from suspended growth systems are accurate predictors of attached growth systems (Grady et al., 1996; Van Loosdrecht et al., 1990).

There are some studies which used biofilm grown cultures to calculate biokinetic parameters, but they measured the biokinetics after disruption of the biofilm structure and then treated the system as a pseudo suspended growth culture (Cao and Alaerts, 1995; Jih and Huang, 1994). However, it is unclear that biokinetic parameters are not affected by disruption of this biofilm structure. I believe

destruction of EPS will affect the biokinetic parameters because there is not a biofilm after destruction.

Several methods have been developed to measure biokinetic parameters from cultures within biofilms. These are presented below.

Bakke et al., (1984) calculated Monod growth kinetic constants using bulk substrate concentrations for steady state biofilms. They concluded that *P. aeruginosa* does not behave differently in a suitable medium, temperature and pH in biofilms than in planktonic cultures.

Rittmann et al., (1986) measured reactor influent and effluent substrate concentrations, then by normalizing these data they defined a series of design curves. Due to the inherent error in the sample analysis and visual comparison, it appears difficult to achieve accurate matches between the design curves and the experimental data (see Rittmann et al., 1986 and Riefler et al., 1998). Thus, the accuracy of the retrieved biokinetic parameters is uncertain.

Nguyen and Shieh, (1995) developed a batch method for determining biokinetic parameters in fluidized bed reactors. In this approach, mass transfer limitations are lumped into the model along with the biokinetic parameters and are not accounted for explicitly. Since biokinetic parameters are not calculated independently, the reliability of the calculated biokinetic parameters were questioned. These values depended on correct estimation of mass transfer parameters, such as diffusivity and external mass transfer coefficient (Riefler et al., 1998).

Zhang and Huck (1996) developed a technique to determine biokinetic and substrate diffusion coefficients in water treatment biofilm systems. Basically they

operated their reactor at different steady states and used steady-state biofilm equations developed by Rittmann and McCarty (1980). They determined the diffusion coefficient for substrate in water, the minimum substrate concentration to maintain a steady-state biofilm, and the half-saturation coefficient. Because of the assumptions used in the model, the sensitivity of measurements limited final accuracy of their approach.

Samb et al., (1998), Reifler et al., (1998) and Cheton et al., (2001) used a respirometric technique, integrated with a unsteady state diffusion + reaction model, and predicted Monod growth constants. However, these authors did not verify the assumptions used in their models.

In summary, the techniques presented above are limited. First, because some of these studies rely on measuring concentrations at steady-state conditions, long time periods are needed to bring the systems back to steady state between tests. These studies defined steady state in terms of substrate concentration, however, none of them considered biofilm structure dynamics. It is expected that the biofilm structure will not reach steady state (Figure 1.12) although substrate concentrations may reach pseudo steady state. Second, the techniques using previously developed biofilm models suffer from the accuracy of parameters (not directly measured) in the models such as effective diffusivity, biofilm density, external mass transfer coefficient, etc. Most of the biofilms grown under liquid flow have heterogeneous structure and these parameters show local variability (Yang and Lewandowski 1995). None of the above studies considered such biofilm structure in their model. A third problem is that none of these studies verified their results (not tested under different operation conditions).

The developed models predict biokinetic coefficients using a fitting technique. The iterations continue until experimentally measured bulk concentration and/or flux mathematically are calculated. All these models somehow predict substrate concentration profiles in biofilms, but predicted and experimental concentration profiles were never compared!

To overcome these problems, first we need to examine what happens to substrates in the biofilm. Substrates form concentration profiles in biofilms and substrate concentration decreases toward the bottom, because of mass transfer limitations and microbial consumption. For that reason bulk concentrations cannot represent true substrate concentrations in biofilms and it is important to use biokinetic parameters and concentrations directly determined in biofilms. This can be accomplished only by using concentration profiles from microelectrode measurements in biofilms.

Lewandowski et al., (1991) noticed the problems explained above and developed a method to calculate biokinetics parameters for biofilms. They exemplified the method by calculating biokinetic parameters from dissolved oxygen concentration profiles measured across a biofilm. The technique, however, was applicable to only the Monod kinetics and the computational procedures employed were performing well only at low dissolved oxygen concentrations, near the half saturation concentration for oxygen.

In other reports, addressing similar problems, Berg et al., (1998) developed a method of predicting substrate concentration profiles from reaction rates in different zones in the sediments. By increasing the number of reaction zones, they successfully

predicted the concentration profiles of  $\text{NO}_3^-$ ,  $\text{O}_2$ , using Nelder and Mead 's (1965) down hill simplex method. Even though the application of this method to biofilms is difficult, the authors showed that the simplex method could be used to predict substrate concentration profiles, and their approach could, in principle, be used in biofilms. Similarly, in Robinson (1985)'s review paper about determining microbial kinetic parameters using nonlinear regression analysis, he mentioned that simplex algorithm is superior to Gaussian methods. Many of the techniques used in nonlinear regression, such as Levenberg-Marquart method, are modified versions of the Gaussian method (Robinson 1985).

Visser et al., (2002), also at the Center for Biofilm Engineering, used the Levenberg-Marquart algorithm along with least squares estimates to find biokinetic parameters by minimizing the least squared differences between experimental data and the model prediction. The authors used MATLAB's *leastsq routine* (in version 6.1 it is called *lsqnonlin*), which requires good guesses of the initial values, and for these reason Visser et al., (2002) had to define a method to select initial values to reduce the number of iterations. Moreover, their method did not allow predicting concentrations at *exactly* the same location as obtained by microsensor measurement location. To overcome this problem they used an interpolation technique (the cubic spline interpolation option in MATLAB), which added unknown errors to the solution. Although this method has the problems stated above, it might be used for the purpose of quantifying biokinetic parameters in biofilms. However, this method and computer program is not generally available.

The quantification of biokinetic parameters from microelectrode data is possible from the solution of the diffusion reaction model of biofilm. The steady state diffusion-reaction equation, including a maintenance factor through, a biofilm in one dimension is given by the following nonlinear differential equation:

$$D_{\text{eff}} \frac{d^2S}{dx^2} = \frac{\mu X_f}{Y_{x/o}} + m X_f \quad (1.16)$$

The following assumptions were made with respect to equation 1.16.

1. The growth limiting substrate is oxygen.
2. The biofilm is uniform.
3. The substrates in the biofilm are transported only via diffusion and described according to Fick's law .
4. The biofilm density and diffusivity can be represented by their average values.
5. Mass transfer of oxygen is one-dimensional only.
6. The biofilm (in terms of oxygen consumption rate) is at pseudo steady state.

It is also assumed, the specific growth rate,  $\mu$ , can be described by one of growth models (Equations 1.5, 1.6, 1.7, or 1.9). None of the previous studies were tested to calculate biokinetics parameters for growth models other than Monod, and did not include maintenance factor for substrate consumption. The biokinetic parameters for growth models other than Monod, including a maintenance factor for substrate consumption, can be calculated using the following hypothesis:

Hypothesis 4. The statistically optimum model to represent *Leptothrix discophora* SP-6 growth in the biofilm form can be determined by an algorithm, developed by the author, which optimizes parameters.

To address this hypothesis, I had the following specific research goals: 1) Produce experimental data from which biokinetic parameters could be calculated. 2) Verify the assumptions stated above. 3) Develop a superior method to calculate biokinetic parameters. 4) Test the different biokinetic models and find the best representative model. For these purposes, I constructed dissolved oxygen microelectrodes and measured oxygen concentration profiles in repeated experiments. I used a specifically designed biofilm system which satisfied the assumptions used in the model.

Hypothesis 5. The physiology and species composition of biofilm systems are expected to be different than suspended growth systems. It has not been proven experimentally that biokinetic parameters from suspended growth systems are accurate predictors of attached growth systems (Grady et al., 1996; Van Loosdrecht et al., 1990). To test this expectation experimentally, I hypothesized that;

*Leptothrix discophora* SP-6 has different growth and substrate consumption kinetics in planktonic and biofilm form.

To address hypothesis 5, I compared microbial growth models and corresponding parameters for planktonic and biofilm systems as determined from hypotheses 4 and 5. The hypothesis is addressed in chapter 4.

## Experimental Methods

### Passive Film Examination

Stainless Steel Coupon Preparation. Type 316S stainless steel coupons (1.6 cm outer diameter) were punched from 1 mm sheet metal (composition given in Table 1.1). Coupons were epoxy embedded in polycarbonate holders using a slow hardening epoxy (Buehler Epoxide). Figure 1.13 illustrates a mounted steel coupon. The holders were constructed from a hollow polycarbonate tube approximately 10 cm long and 0.9 cm inner, and 1.9 cm outer diameter, respectively. Each application of epoxy/glue was allowed 24 hours to harden. All the coupons were polished using 240, 360, 400 and 600 grit size sand papers, followed by fine polishing with 5.0-, 0.3-, and 0.05-micron  $Al_2O_3$  particles placed on micro cloths. Following the mounting on the polycarbonate coupon holders, the electrical connections were made by attaching a copper wire (spring) to the back of each coupon. The contact resistances of the coupons were measured to make sure that the values were less than 1 ohm. The coupons were sterilized in ethyl alcohol solution under the biohood for three hours before placing in sterilized growth medium.

Table 1.1. The composition of 316L stainless steel used in this study ( % w/w).

Fe	Cr	Ni	Mo	Mn	Si	P	N	C	S
69.3	16.4	10.1	2.10	1.71	0.39	0.03	0.03	0.01	0.00
4	9	9				4		7	1

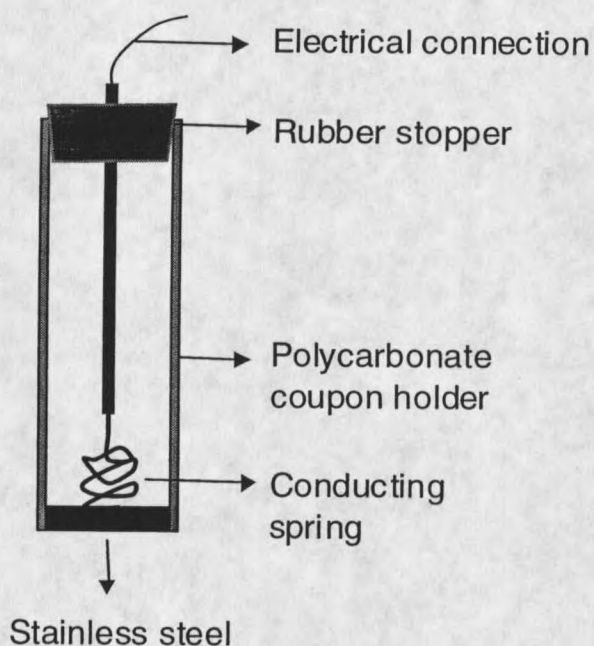


Figure 1.13. Polycarbonate coupon holder and accessories.

Ennoblement Experiments. A stock culture of manganese oxidizing bacteria *Leptothrix discophora* SP-6 was obtained from American Type Culture Collection (ATCC no. 51168). The organisms were grown in a mineral-salt-pyruvate-vitamin (MSPV) medium (ATCC no. 1917). The composition of the MSVP medium is given in Table 1.2. The organisms were centrifuged and re-suspended in MSVP medium containing 20% glycerol and preserved in a freezer at  $-70^{\circ}\text{C}$ . These stock cultures were used to inoculate the reactor.

Table 1.2. ATCC Culture Medium 1917 MSVP for *Leptothrix discophora* SP-6.

(NH <sub>4</sub> ) <sub>2</sub> SO <sub>4</sub>	0.24 g
MgSO <sub>4</sub> ·7H <sub>2</sub> O	0.06 g
CaCl <sub>2</sub> ·2H <sub>2</sub> O	0.06 g
KH <sub>2</sub> PO <sub>4</sub>	0.02 g
Na <sub>2</sub> HPO <sub>4</sub> ·7H <sub>2</sub> O	0.06 g
HEPES	2.383 g
FeSO <sub>4</sub> 10 mM	1.0 mL
Distilled water	984 mL

Adjust to pH 7.2 with NaOH or H<sub>2</sub>SO<sub>4</sub>. Autoclave at 121°C for 15 minutes. Cool to approximately 50°C and aseptically add 1.0 mL of the following filter-sterilized solutions:

20% Sodium pyruvate  
Vitamin solution (see below)

Biotin	20.0 mg
Folic acid	20.0 mg
Thiamine HCl	50.0 mg
D-(+) -calcium pantothenate	50.0 mg
Vitamin B12	1.0 mg
Riboflavin	50.0 mg
Nicotinic acid	50.0 mg
Pyridoxine HCl	100.0 mg
p-Aminobenzoic acid	50.0 mg
Distilled water to	1.0 L

The coupons, prepared as described above (up to 8 coupons) were then placed into the autoclaved (1 atm, 30 minutes) polycarbonate reactor with 500 mL- solution containing MSVP medium, but excluding FeSO<sub>4</sub> (FeSO<sub>4</sub> is only used in stock culture preparations). Manganese was added as MnSO<sub>4</sub> (0.2 mM) using a sterile syringe filter. The reactor (Figure 1.14) was 11 cm inner diameter and 10 cm high. The reactor was continuously aerated via a glass tube. The inlet air and outlet air were filter sterilized. A glass tube (1 mm diameter) with a porous glass tip was placed into

the reactor before autoclaving. We added 0.1 g/L autoclaved agar containing 0.1 M  $\text{Na}_2\text{SO}_4$  into the glass tube which provided a salt bridge for reference electrode. The reference electrode was placed at the end of agar layer immersed into the saturated KCl solution. This method of reference electrode positioning was recommended by Olesen (2000a,b) because direct insertion of a reference electrode into the medium caused  $\text{Cl}^-$  ion leakage into the solution. We used Saturated Calomel Electrode (SCE) as the reference electrode.

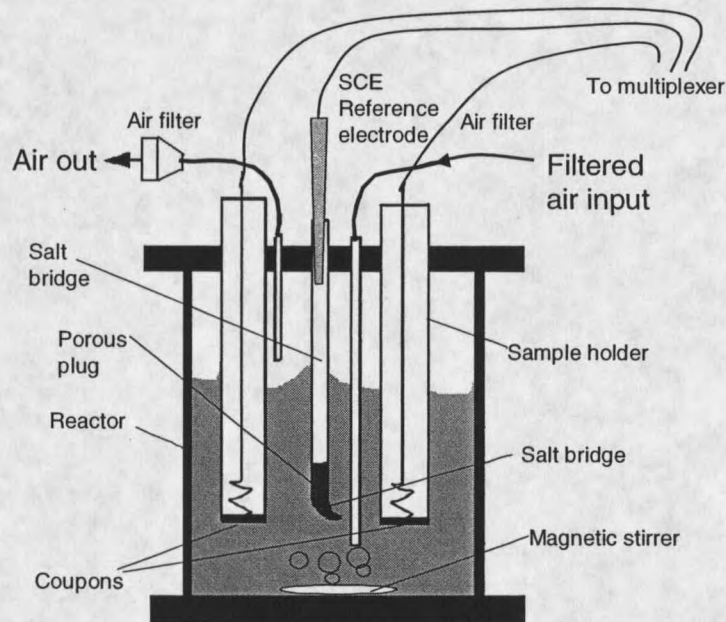


Figure 1.14. The reactor used to ennoblement experiments.

Potentials between SCE and coupons were measured hourly by a data acquisition system (Hewlett Packard 3497A multiplexer connected to a computer) against an SCE. A photograph of reactor and data acquisition system is shown in

Figure 1.15. After at least 6-7 days, the OCP reaches a stable reading,  $\sim +350 \text{ mV}_{\text{SCE}}$ . At this time the coupons are considered ennobled and are removed from the reactor and taken for analysis immediately.



Figure 1.15. A photograph of the reactor and data acquisition system.

Coupon Classifications for Different Experiments. All the coupons were first subjected to the polishing and cleaning procedure described above. The XPS, ToFSIMS and anodic polarization experiments were conducted on five groups of coupons, four of which served as controls. The first group of coupons was subjected to a series of *Leptothrix discophora* SP-6 induced ennoblement processes as described above. These coupons are called as “*ennobled*”. One of the four groups of control coupons was composed of *as-received* coupons, subjected only to the polishing and cleaning procedure described above. The second group of control coupons was immersed into pure sterile water for the same period of time as the other

control coupons. The XPS and ToFSIMS experiments conducted on the two groups of coupons described above serve as the background measurements with respect to which other results were compared. The third group of control coupons was treated with sterile MSVP and a 0.2 mM  $\text{Mn}^{2+}$  solution without any bacteria (herein termed *growth medium treated coupon*) in order to determine the effect, if any, of the growth medium on the stainless steel passive film. The fourth group of control coupons was exposed to MSVP and the bacteria solution without any  $\text{Mn}^{2+}$  (called *biofilm treated coupons*) in order to determine the effect of bacteria on the passive film without the  $\text{Mn}^{2+}$  ions in the medium. Prior to XPS and ToFSIMS analysis, coupons were wiped or rinsed, as explained below in detail, and then the coupons were removed from the polycarbonate holders mechanically, making sure that no epoxy was left on back of the coupons before inserting them in the UHV chamber.

Anodic polarization experiments were performed using as-received, biofilm treated and ennobled coupons.

XPS Analysis. XPS experiments were performed using a PHI Model 5600ci MultiTechnique system located in ICAL laboratory, Physics, MSU. A monochromatized Al K alpha (1486.6 eV) x-ray source was used. An 800-micron diameter equivalent area of the sample surface was analyzed while a  $3 \times 3 \text{ mm}^2$  area was sputtered using  $\text{Ar}^+$  ions for each cycle of depth profiling. In the sputtering process,  $\text{Ar}^+$  ions, accelerated to  $\sim 2 \text{ keV}$  at  $0.25 \text{ }\mu\text{A}$  current, were used to bombard the sample surface for selected time intervals ( $\sim 0.5 \text{ min}$ ) until Fe and Cr oxides were removed and metallic Fe and Cr (bulk SS) were shown to be present. Following each

cycle of sputtering, multiplex XPS spectra of selected core level emissions were taken to determine the depth profiles of Mn, Fe, C, O and Ni for each of the control and the ennobled coupons. Ni depth profile was omitted in the figures because of low Ni concentration in the passive film and because no variation with any treatment was observed in the Ni profile.

ToFSIMS Experiments. A Phi-Evan's Trift-I system, located in the ICAL laboratory, Physics, MSU, was used for the ToFSIMS experiments. The system consists of a liquid metal ( $\text{Ga}^+$ ) ion gun for obtaining high mass and high spatial resolutions for chemical imaging. In these experiments 25 keV  $\text{Ga}^+$  primary ions were used to generate secondary ions. These ions are separated and detected by a triple-pass  $90^\circ$  spherical sector electrostatic mass analyzer. The output is a high-resolution mass spectrum plotted as a function of intensity vs. mass-to-charge ratio. For chemical maps a  $256 \times 256$  pixel area (typically corresponding to a  $120 \times 120$  square micron size) with each pixel containing the full mass spectrum was stored in the computer media as raw files. Chemical maps of Fe, Cr and Mn (Ni was omitted for the same reason as explained above) were extracted retrospectively following the raw data acquisition.

Measurement of Pitting Corrosion. Anodic polarization experiments were conducted using a potentiostat/galvanostat (EG&G Princeton Applied Research, model 273A) with two graphite electrodes and an SCE as reference placed into an electrochemical cell (Figure 1.16). The 352 SoftCorr III corrosion measurement

software (EG&G, Princeton Applied Research) was used to set up anodic polarization processes. OCPs were measured before each experiment, versus the SCE using a handheld multi meter (Wavetek DM23XT, internal resistance 10m $\Omega$ ).

Pitting potentials of the 316L stainless steel coupons were obtained through potentiodynamic polarization. Scans were initiated 10 mV below the OCP and scanned, using a scan rate of 5mV/s, to 0.8 V<sub>SCE</sub> or 1mA, whichever was reached first. Experiments were conducted at room temperature in 0.1M Na<sub>2</sub>SO<sub>4</sub> solutions with NaCl at different concentrations.

Anodic polarization is mostly used to understand corrosion behavior of metals (Silverman 1998). The anodic polarization technique requires a three electrode system: 1) a working electrode: the metal to be tested, 2) a counter electrode: platinum or graphite are generally used ones, and 3) a reference electrode. These three electrodes are connected to a potentiostat. The potentiostat is used 1) to apply potential between working electrode and reference electrode, 2) to measure current between counter electrode and working electrode, 3) to set a range of potential to be tested, and 4) to set the scan rate (or the rate potential variation by time). The electrochemical cell used in anodic polarization experiment is given in Figure 1.16. A computer is used to control the potentiostat.

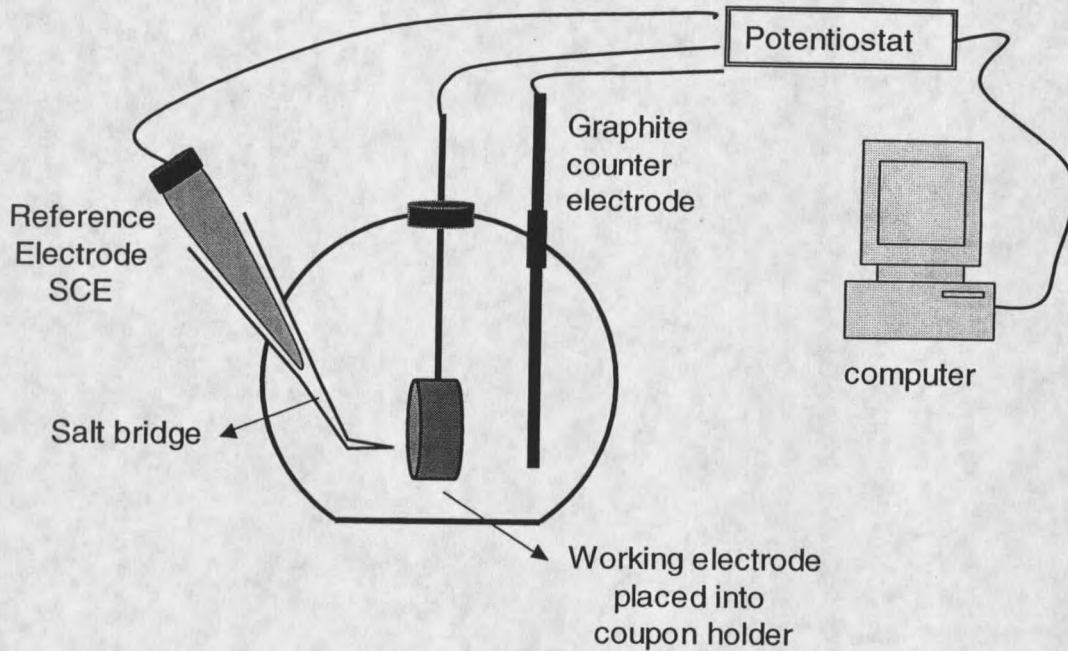


Figure 1.16. The electrochemical cell used for anodic polarization consisted of three electrodes, a potentiometer, and a computer.

The test coupons were placed into a specifically designed coupon holder. The electrochemical cell is filled with the electrolyte solution depending on the measurement.

For a stainless steel coupon used in this study a typical anodic polarization curve is presented in Figure 1.17.

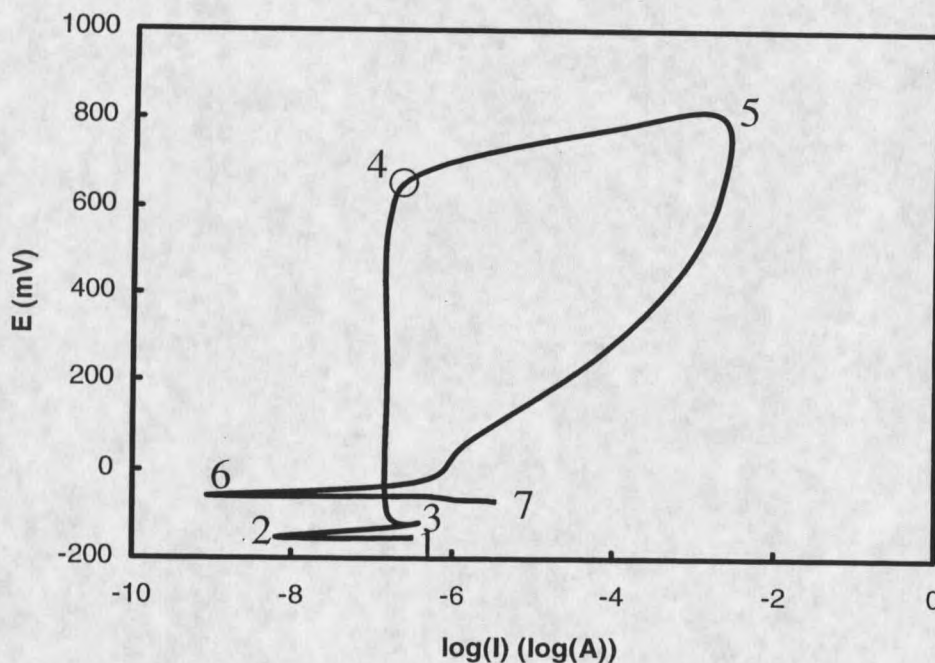


Figure 1.17. A typical anodic polarization curve.

The y axis is logarithm of the measured current between working electrode and counter electrode with a unit of ampere. The point 1 is corrosion potential or OCP of the stainless steel sample. Potential is applied from the point 1. From points 1 to 2, the current decreases with slightly increased potential because of the proximity of the metal's OCP. The point 2 is OCP of the stainless steel, since OCP measured in the medium the potentials at points 1 and 2 are almost the same ( $\pm 10\text{mV}$ ). Between points 2 and 3, the current increases with increased potential, and metal begins to corrode like an active metal until the potential reaches a critical value where the current becomes almost constant (point 3). At this stage, the current does not change with increased potential (which shows passive film formation) until point 4. The

oxide layer prevents diffusion of chloride ions through passive layer. With increased potential the passive film breaks down at the point 4 and suddenly current starts to increase significantly. The potential at point 4 is called the pitting potential, as the passive film breaks down and ions attack metals. The pitting potential is the minimum potential at which active pitting will began. Any potential above the pitting potential will open active pits on metal's surface. The point 5 is end of the forward scan, and is set by the user. After point 5 the backward scan is started. If the passive film was not compromised, the backward scan will pass the left side of forward scan, indicating increased resistance to corrosion by increased passive film thickness. If the passive film has been compromised, the backward scan will fall on the right side of the forward scan, as seen in Figure 1.17. As the potential continues decreasing, the metal will repassivate by forming oxide layer and will lower the current. The point 6 represents the repassivation potential. The repassivation potential shows the potential at which initiation of pit may begin. The point 7 is the end of the cycle.

The pitting potential measured from anodic polarization curves are functions of temperature, scan rate, pH, mixing rate, and chloride concentration. For these reasons, the same conditions for anodic polarization experiments were maintained throughout. All anodic polarization experiments were performed at room temperature (25 °C) and repeated at least four times to produce a representative data (Burstein and Ilevbare 1996).

### Planktonic Growth Kinetic Measurements

Chemostat. The microorganisms were grown in a New Brunswick (BioFlo 2000) chemostat with a working volume of 2 L, equipped with pH, agitation, and temperature controllers as shown Figure 1.18. The sensitivities of the control units for pH, temperature and agitation rate were respectively: 0.1 unit, 0.1 °C, and  $\pm 1$  rpm. Prior to use, the chemostat, including growth medium, filters, and tubings, were autoclaved for 30 minutes at 121°C. The pH was controlled by pumping solutions of 0.2 N NaOH and 0.2 N H<sub>2</sub>SO<sub>4</sub>. The solution in the chemostat was stirred by a blade type double impeller at 350 rpm. The dissolved oxygen electrode is calibrated by saturating with air and sparging the reactor with nitrogen (zero oxygen). The dissolved oxygen concentration was controlled by sparging filtered air or filtered mixtures of air + pure oxygen or air + nitrogen in various proportions, depending on the needs, at the flow rates between 1 L/h and 5 L/h.

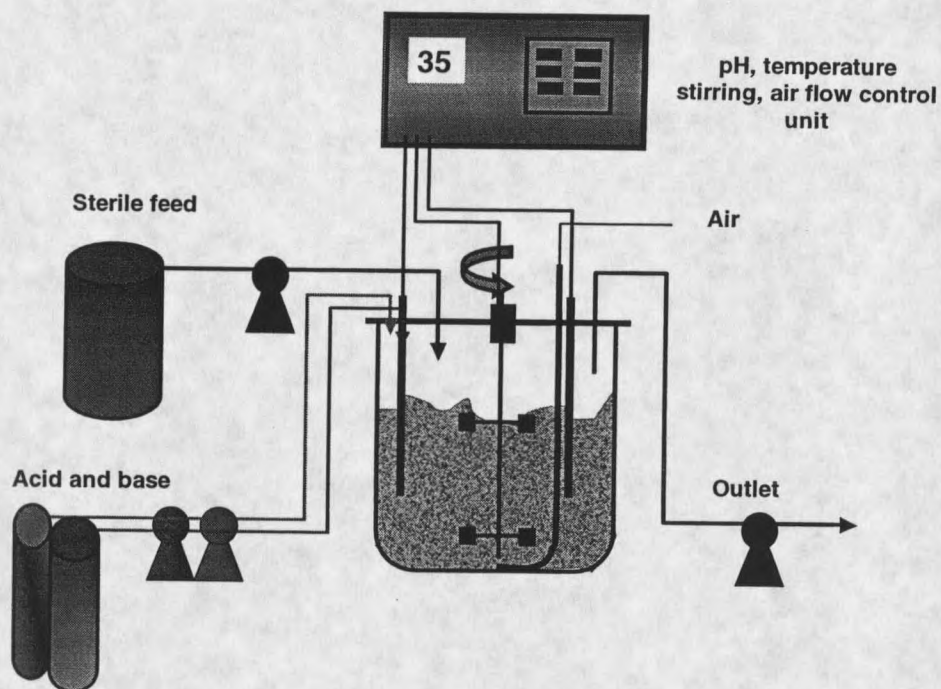


Figure 1.18. Schematic diagram of chemostat used in this study.

### Biofilm Growth Kinetic Measurements

Colony Biofilms. The colony biofilms of *Leptothrix discophora* SP-6 were prepared according to the procedure described by Anderl et al., (2000). Forty-eight hour old cultures of *Leptothrix discophora* were diluted to an optical density of 0.02 at 600 nm (using 1-cm path length) in growth medium. Ten  $\mu\text{L}$  of diluted culture was used to inoculate one sterile, polycarbonate membrane filter (25 mm ID, 0.2 micron pore size) lying on agar plate. The membrane filters were sterilized by UV light for 15 min for each side prior to inoculation. The Petri plates were kept at room

temperature and the membrane filters were transferred to fresh agar plates every 12 h. The growth substrates were supplied by the agar, and transferred through the membrane to the colony biofilm. The oxygen required for growth was transported from air to the colony, and all substrates were transported via diffusion. A schematic diagram of colony biofilm is presented in Figure 1.19.

To grow the biofilms, we used ATCC Culture 1917 MSVP for *Leptothrix discophora* SP-6 (American Type Culture Collection Catalogue, 1992). It consisted of 0.24 g  $(\text{NH}_4)_2\text{SO}_4$ , 0.06 g  $\text{MgSO}_4 \cdot 7\text{H}_2\text{O}$ , 0.06 g  $\text{CaCl}_2 \cdot 2\text{H}_2\text{O}$ , 0.02 g  $\text{KH}_2\text{PO}_4$ , 0.06 g  $\text{Na}_2\text{HPO}_4 \cdot 7\text{H}_2\text{O}$ , and 2.383 g HEPES in 950 mL distilled water. The pH of this medium was adjusted to 7.2 with NaOH or  $\text{H}_2\text{SO}_4$ . We added 15 g Agar Noble (Difco 214230) and autoclaved this solution at 121 °C for 15 minutes (for 1 L volume of the solution); after cooling it to approximately 50 °C, we added 1 mL vitamin solution (see below), 1 mL  $\text{FeSO}_4$  (10 mM) and 48 mL of pyruvate solution (at different concentrations) aseptically by filter-sterilizing (0.2 micron sterile syringe filter, Corning, 431219). One L of vitamin solution consisted of 20 mg Biotin, 20 mg Folic acid, 50 mg Thiamine HCl, 50 mg D-(+) -calcium pantothenate, 1 mg Vitamin B12, 50 mg Riboflavin, 50 mg Nicotinic acid, 50 mg Pyridoxine HCl, 50 mg p-Aminobenzoic acid. After adding vitamin solution, we poured this solution into sterilized petri dishes and kept these dishes in a clean and cold place.

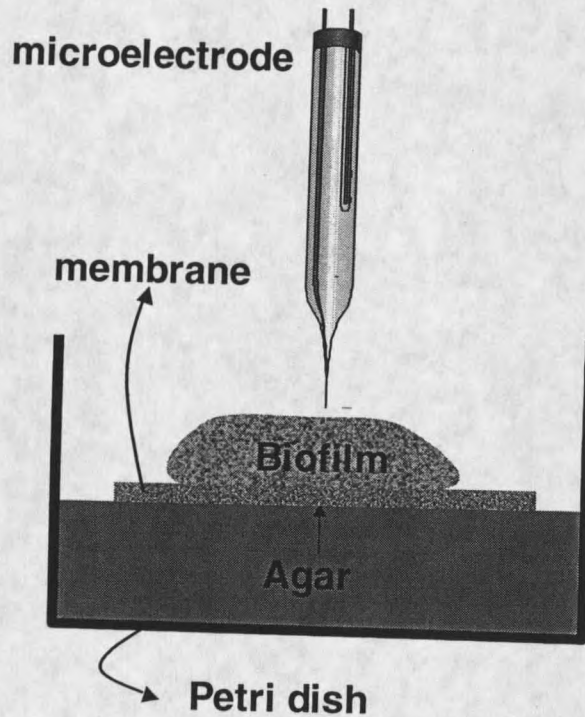


Figure 1.19. Diagram of a colony biofilm grown on top of a membrane filter. The growth substrate is supplied by the agar and transferred through the membrane to the biofilm. The microorganisms receive oxygen from the air.

Dissolved Oxygen Microelectrode Measurements. Dissolved oxygen concentration profiles were measured using Clark type microelectrodes with a guard cathode, as described by Revsbech, (1986). Details of the construction process is presented in the Center for Biofilm Engineering microsensors workshop materials (Microsensors – Workshop, Center for Biofilm Engineering, August 2001). The microelectrodes had tip diameters less than  $10\ \mu\text{m}$  to prevent damaging the biofilm structure during measurements. The oxygen concentrations were measured at  $5\ \mu\text{m}$  intervals. The response time of the microelectrodes was less than 0.3 s. The

microelectrodes were calibrated using air and pure nitrogen gases in tap water. The calibrations before and after the measurements were within the range of acceptable experimental error. Figure 1.20 shows schematic diagram of a dissolved oxygen sensor used in this study.

To measure dissolved oxygen concentration, a -0.8 V is applied between the cathode (Pt) and anode (Ag/AgCl wire) and the current is measured between them. A HP 4140B pA meter / DC voltage source was used to measure the current. The measured current is directly proportional to the oxygen concentration in the vicinity of the microelectrode tip. The data is collected and the microelectrode can be moved simultaneously using a custom written software package known as Vscan.

Microelectrodes were mounted on a micromanipulator (Model M3301L, World Precision Instruments, New Haven, CT) equipped with a stepper motor (Model 18503, Oriel, Stratford, CT) controlled by the Oriel Model 20010 interface. The microelectrode was introduced to the biofilm from the top perpendicular to the biofilm. The stepper motor was interfaced with a computer, and the microelectrode movement was handled by a controller (CTC-283-3, Micro Kinetics) with a positioning precision of 0.1  $\mu\text{m}$ . Custom software was used to control and to coordinate microelectrode movement and the data acquisition. The position of the microelectrode was monitored using a stereo microscope (Leica Stereo Zoom 7) at 40 – 70 times magnification.

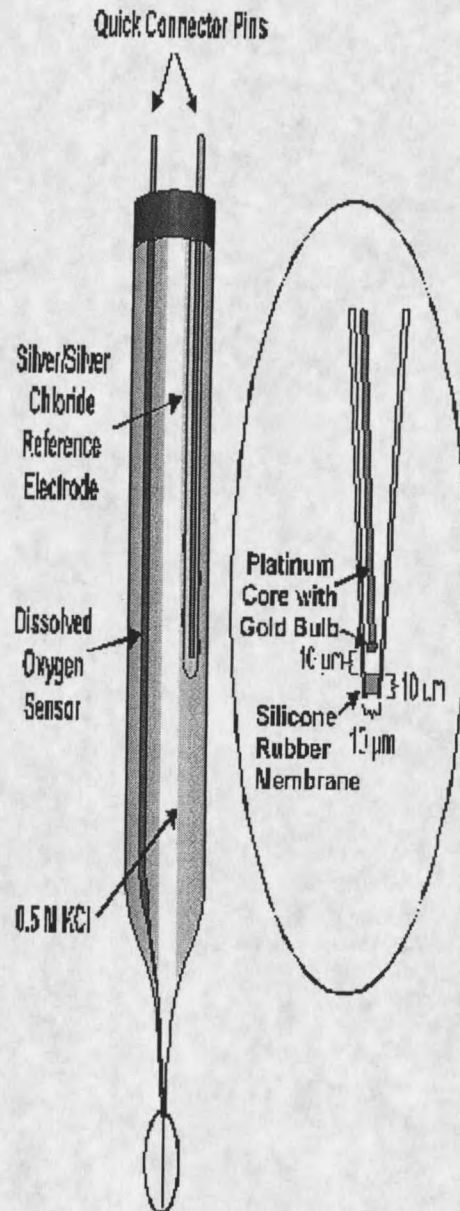


Figure 1.20. Schematic diagram of a Clark type dissolved oxygen sensor. The insert shows the position of the cathode, the reference electrode, and the silicone rubber membrane.

## CHAPTER 2

BIOMINERALIZED MANGANESE DEGRADES PASSIVE FILMS AND  
LOWERS PITTING POTENTIAL OF STAINLESS STEEL 316L

Nurdan Yurt<sup>1,2</sup>, Recep Avci<sup>3</sup>, Zbigniew Lewandowski<sup>1,4</sup>, John Sears<sup>1,2</sup>

1. Center for Biofilm Engineering, Montana State University, EPS 366, Bozeman,  
MT 59717
2. Chemical Engineering, Montana State University, 306 Cobleigh Hall, Bozeman,  
MT 59717
3. Department of Physics, Montana State University, EPS 254, Bozeman, MT  
59717
4. Civil Engineering, Montana State University, EPS 366, Bozeman, MT 59717

---

Part of this paper has been presented in NACE 2002 conference. The paper is prepared for submission to Corrosion Science.

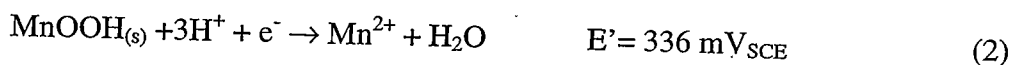
Abstract

The effect of ennoblement of 316L stainless steel by biomineralized manganese deposits on chemistry of passive films was studied using surface-sensitive analytical techniques and cyclic polarization. Under well-defined laboratory conditions, stainless steel coupons were ennobled to  $\sim +350\text{mV}_{\text{SCE}}$  by biofilms of manganese-oxidizing bacterium *Leptothrix discophora* SP-6. Passive films on the ennobled coupons were analyzed by x-ray photoelectron spectroscopy (XPS) and time-of-flight secondary ion mass spectroscopy (ToFSIMS). From the XPS depth profiles of Fe, Cr, O, Ni, C and Mn, we evaluated thickness of the passive layers before and after ennoblement, while from the ToFSIMS depth profiles, spatial distribution of Mn, Cr, Fe, and Ni on the metal surface were evaluated. Because the ennobled coupons were covered with biomineralized deposits, the deposits were removed by sputtering in ultrahigh vacuum (UHV) before probing the chemistry of the underlying passive layers. The results show that oxide layers on the ennobled coupons are thinner than those on the pre-ennobled coupons. Pitting potentials in 0.2 M NaCl for as received, polished clean coupons and biofilm covered coupons (non-ennobled) were  $573 \pm 67 \text{ mV}_{\text{SCE}}$  and  $497 \pm 64 \text{ mV}_{\text{SCE}}$ ; in contrast the ennobled coupons pitted spontaneously in 0.2 M NaCl solution. We conclude that the biomineralized deposits degraded the quality of the passive film on stainless steel coupons by reducing its thickness and lowering the pitting potential.

### Introduction

Numerous studies have reported that the open circuit potentials (OCP) of stainless steels immersed in natural waters shift spontaneously in the noble direction from  $-200 \text{ mV}_{\text{SCE}}$  to  $+350 \text{ mV}_{\text{SCE}}$ . This process is known as *ennoblement* and may facilitate pitting corrosion in the presence of aggressive ions such as  $\text{Cl}^-$  even at low concentrations that do not cause pitting of non-ennobled coupons (Amaya and Miyuki 1997; Linhardt 1996; Suleiman et al., 1994; Felder 1990).

Several mechanisms have been proposed to explain ennoblement: They include enzymatic depolarization of the oxygen reduction reaction (Mollica et al., 1990; Scotto et al., 1985), strong acidification of the surface as a result of microbial activity in biofilms (Chandrasekaran and Dexter 1993; Little et al., 1990), combined effects of increased  $\text{H}_2\text{O}_2$  concentrations and decreased pH, both biologically originated (Feron et al., (1997), and reduction of  $\text{MnO}_2$  deposited by manganese-oxidizing microorganisms. This latter mechanism of ennoblement is the only one that has been verified experimentally in the laboratory as well as in the field (Broughton et al., 2001; Olesen et al., 2000; Linhart 1996; Dickinson and Lewandowski 1996). According to this mechanism, the microbiologically deposited  $\text{MnO}_2$  is electrochemically reduced to  $\text{MnOOH}$ , and then further to  $\text{Mn}^{2+}$ . Reactions (1) and (2) illustrate this mechanism. Note that these reactions have the same electrode potential ( $E'$ ) as that of the 316L stainless steel coupons ennobled in the laboratory and in the field.



The net reaction is:



Where  $\text{pH}=7.2$ ,  $[\text{Mn}^{2+}] = 1 \times 10^{-6} \text{ M}$ .

Unexpected pitting of microbially ennobled stainless steel has been reported. For example, Olesen et al., (2001) showed that 304L stainless steel coupons ennobled by the biomineralized deposits pitted at 0.35 % NaCl concentration, which is generally not sufficient to cause pitting. In another study, Neville and Hodgkiss (2000) correlated passive film composition with corrosion resistance and demonstrated that a thicker passive film makes stainless steel more corrosive resistant. Combining these two factors, we hypothesize that microbial ennoblement of stainless steel degrades the passive film and, therefore, can cause pitting of stainless steels immersed in low chloride solutions, e.g., fresh waters.

To test this hypothesis we have quantified the effect of ennoblement on the chemistry of passive layers on 316L stainless steel. Using coupons that are 1) polished as received, 2) ennobled, and 3) biofilm covered (but not ennobled), we measured pitting potentials and passive film thickness to relate the chemistry of passive layers to the susceptibility to corrosion.

To quantify the chemistry and thickness of passive films, we used XPS and ToFSIMS to determine the atomic concentration profiles of such elements as Fe, Cr, Ni, O and Mn with micron-scale resolution. Pitting potentials were measured in 0.2 M NaCl solution, as 316L stainless steel normally does not pit in 0.2 M NaCl. To enoble 316L stainless steel coupons, we used biofilms of manganese-oxidizing bacterium *Leptothrix discophora* SP-6. Measurements were repeated to determine average chemical composition of the passive films and average pitting potentials.

### Materials and Methods

#### Ennoblement Experiments

A stock culture of MOB *L. discophora* SP-6 was obtained from the American Type Culture Collection (ATCC no. 51168). The organisms were grown in a mineral-salt-pyruvate-vitamin (MSPV) medium (ATCC no. 1917), Table 2.1. The organisms were harvested by centrifuging, re-suspended in the MSVP medium containing 20% glycerol, and stored in a freezer at  $-70^{\circ}\text{C}$ . These stock cultures were used to inoculate the reactor, which contained 316L stainless steel coupons.

Table 2.1. ATCC Culture Medium 1917 MSVP for *Leptothrix discophora* SP-6.

(NH <sub>4</sub> ) <sub>2</sub> SO <sub>4</sub>	0.24 g
MgSO <sub>4</sub> ·7H <sub>2</sub> O	0.06 g
CaCl <sub>2</sub> ·2H <sub>2</sub> O	0.06 g
KH <sub>2</sub> PO <sub>4</sub>	0.02 g
Na <sub>2</sub> HPO <sub>4</sub> ·7H <sub>2</sub> O	0.06 g
HEPES	2.383 g
FeSO <sub>4</sub> 10 mM	1.0 mL
Distilled water	984 mL

Adjust to pH 7.2 with NaOH or H<sub>2</sub>SO<sub>4</sub>. Autoclave at 121°C for 15 minutes. Cool to approximately 50°C and aseptically add 1.0 mL of the following filter-sterilized solutions:

20% Sodium pyruvate

Vitamin solution (see below)

Biotin	20.0 mg
Folic acid	20.0 mg
Thiamine HCl	50.0 mg
D-(+)-calcium pantothenate	50.0 mg
Vitamin B12	1.0 mg
Riboflavin	50.0 mg
Nicotinic acid	50.0 mg
Pyridoxine HCl	100.0 mg
p-Aminobenzoic acid	50.0 mg
Distilled water to	1.0 L

Type 316L stainless steel coupons (composition given in Table 2.2) were polished, sonicated in acetone, and mounted in holders made of polycarbonate tubes using a slow-hardening epoxy resin. The coupons, 1.6 cm in diameter, mounted in the polycarbonate coupon holders, were polished using 240, 360, 400 and 600 grit size sandpapers, followed by fine polishing with 5.0-, 0.3-, and 0.05-micron Al<sub>2</sub>O<sub>3</sub> particles placed on microcloths. Electrical connections between the coupons and the external circuit were made by attaching a copper wire to the back of each coupon, within the holder, and extending the wire beyond the coupon holder. Contact resistances of the coupons were measured, and the coupons were accepted only if these values were less than 1 ohm. The coupons in their holders were sterilized in 95% ethyl alcohol under the biohood for three hours, and placed into the autoclaved polycarbonate 500 mL-reactor containing MSVP medium without FeSO<sub>4</sub> (FeSO<sub>4</sub> was

used only to preserve the stock culture). Manganese was added to the reactor as  $\text{MnSO}_4$  (0.2 mM) using a sterile syringe filter. Potentials were measured hourly against the saturated calomel electrode (SCE). After 6-7 days, when the OCP stabilized at  $\sim +350 \text{ mV}_{\text{SCE}}$ , holders with the coupons were removed from the reactor and the coupons were subject to surface analysis. The coupons were divided into five groups depending on the treatment;

- Group I : Working coupons (ennobled)
- Group II : As received coupons
- Group III : Sterile DI water treated coupons
- Group IV : Growth medium treated coupons (MSVP and  $\text{Mn}^{2+}$ )
- Group V : Biofilm treated coupons (MSVP and bacteria)

The working coupons (group I) were ennobled by the MOB, as described above. As received coupons (group II) were polished and cleaned by the procedure described above. Group III coupons were immersed in the sterile DI water for the same period of time as the other control coupons (6-7 days). Growth medium treated coupons (group IV) were exposed to sterile MSVP containing 0.2 mM  $\text{Mn}^{2+}$  to determine the effect of the growth medium on the composition of the passive film. Biofilm treated coupons (group V) were exposed to MSVP, growth medium inoculated with the bacteria but without  $\text{Mn}^{2+}$ , to determine the effect of the bacteria alone on the passive film composition. Prior to the XPS and ToFSIMS analyses, the

coupons were wiped or rinsed, then removed from the polycarbonate holders and immediately inserted into the UHV chamber.

Table 2.2. Composition (w/w) of 316L stainless steel.

Fe	Cr	Ni	Mo	Mn	Si	P	N	C	S
69.34	16.49	10.19	2.10	1.71	0.39	0.034	0.03	0.017	0.001

XPS analysis was conducted on samples prepared in two different ways: (1) coupon surfaces were rinsed with DI water and wiped completely with a cotton swab to remove the biomineral deposits, and (2) coupon surfaces were rinsed gently with DI water only, leaving the biomineral deposits on the surface. At least two different areas were analyzed on a given coupon. The motivation for removing the biofilms before analysis (preparation 1) is to determine whether or not substantial changes are introduced to the passive layer as a result of biofilm activity. Such a change usually manifests itself with increased passive layer thickness as compared with the controls (Olefjord et al., 1985). The motivation for leaving the biofilm intact (preparation 2) is to prevent repassivation in case the ennoblement reduces the film thickness and compromises the passive film in such a way that removal of biominerals and exposure to ambient conditions will simply cause the re-oxidation of the surface before one can determine the changes due to ennoblement.























































































































































































































